

SAMMSON fosters cancer cell fitness by concertedly enhancing mitochondrial and cytosolic translation

Roberto Vendramin^{1,2,3}, Yvessa Verheyden¹, Hideaki Ishikawa⁴, Lucas Goedert¹, Emilien Nicolas⁵, Kritika Saraf⁵, Alexandros Armaos⁶, Riccardo Delli Ponti⁶, Keichi Izumikawa⁴, Pieter Mestdagh^{7,8}, Denis L. J. Lafontaine^{1,5}, Gian Gaetano Tartaglia⁶, Nobuhiro Takahashi⁴, Jean-Christophe Marine^{2,3} and Eleonora Leucci^{1*}

Synchronization of mitochondrial and cytoplasmic translation rates is critical for the maintenance of cellular fitness, with cancer cells being especially vulnerable to translational uncoupling. Although alterations of cytosolic protein synthesis are common in human cancer, compensating mechanisms in mitochondrial translation remain elusive. Here we show that the malignant long non-coding RNA (lncRNA) SAMMSON promotes a balanced increase in ribosomal RNA (rRNA) maturation and protein synthesis in the cytosol and mitochondria by modulating the localization of CARF, an RNA-binding protein that sequesters the exo-ribonuclease XRN2 in the nucleoplasm, which under normal circumstances limits nucleolar rRNA maturation. SAMMSON interferes with XRN2 binding to CARF in the nucleus by favoring the formation of an aberrant cytoplasmic RNA-protein complex containing CARF and p32, a mitochondrial protein required for the processing of the mitochondrial rRNAs. These data highlight how a single oncogenic lncRNA can simultaneously modulate RNA-protein complex formation in two distinct cellular compartments to promote cell growth.

Highly proliferating cells, such as cancer cells, have an elevated metabolic demand for protein synthesis¹. The vast majority of proteins is produced in the cytosol and depends on the correct assembly of ribosomes. Ribosome biogenesis requires the activity of all three nuclear RNA polymerases². Whereas the biogenesis of ribosomal proteins is initiated in the nucleus by the RNA polymerase II, maturation of a polycistronic precursor generated by RNA pol I in the nucleolus, gives rise to 18S, 28S and 5.8S rRNAs that are subsequently modified and processed by hundreds of small nucleolar RNAs (snoRNAs) and protein cofactors into their mature forms. The 5S rRNA instead, is transcribed independently in the nucleoplasm by the RNA pol III³.

The synthesis of 13 of the mitochondrial membrane proteins engages a dedicated set of ribosomes, or mitoribosomes, whose biogenesis requires active transcription by the mitochondrial polymerase to produce the mitochondrial rRNAs precursor that is then cleaved by RNase H and p32 to produce the mature 12S and 16S⁴. (Mito)ribosome biogenesis is the most energy-consuming cellular process³ and it is therefore tightly regulated by growth and stress signaling pathways^{5–8}.

Apart from the aforementioned 13 membrane peptides, the majority of the mitochondrial proteome is encoded by the nuclear genome and synthesized in the cytosol as precursor proteins that are ultimately imported into mitochondria⁹. Thus, a fully functional oxidative phosphorylation chain requires proteins translated by

both mitochondrial and cellular machineries. The two translation apparatuses therefore need to be synchronized and tightly regulated to respond to environmental cues in a coordinated fashion. Accordingly, desynchronization through disruptions of mitochondrial protein synthesis impacts cell proliferation and fitness^{10–12}, thus highlighting the existence of intracellular circuit(s) that couple mitochondrial translation to cell proliferation¹³. In yeast, mitochondrial protein synthesis defects cause mitochondrial membrane depolarization thus impairing the import of nuclear-encoded mitochondrial precursors. These accumulate in the cytosol to induce a proteotoxic stress response, known as mitochondrial precursor overaccumulation stress (mPOS)^{14,15}.

Similarly to mitochondrial translation, cytosolic protein synthesis is tightly linked to cell proliferation and under direct control of oncogenes and tumor suppressors¹⁶. Increasing evidence indicates that oncogenes can stimulate the translation rates in the cytosol and mitochondria. However, how cancer cells ensure that the proper balance between the output of the two protein synthesis machineries is maintained remains unclear.

One example of an oncogene with a direct role in control of translation is the transcription factor Myc, which directly increases protein synthesis rates in the cytosol by controlling the expression of multiple components of the protein synthetic machinery¹⁷. Myc is also capable of enhancing the activity of the mitochondrial protein synthesis machinery. p32, a mitochondrial protein required for the

¹Laboratory for RNA Cancer Biology, Department of Oncology, LKI, KU Leuven, Leuven, Belgium. ²Laboratory for Molecular Cancer Biology, Department of Oncology, LKI, KU Leuven, Leuven, Belgium. ³Laboratory For Molecular Cancer Biology, Center for Cancer Biology, VIB, Leuven, Belgium. ⁴Department of Applied Biological Science, Global Innovation Research Organizations, Tokyo University of Agriculture and Technology, Tokyo, Japan. ⁵RNA Molecular Biology, Center for Microscopy and Molecular Imaging, Université Libre de Bruxelles, Charleroi, Belgium. ⁶Centre for Genomic Regulation, University Pompeu Fabra and Catalan Institution for Research and Advanced Studies, Barcelona, Spain. ⁷Center for Medical Genetics, Gent University, Gent, Belgium. ⁸Cancer Research Institute Gent, Gent University, Gent, Belgium. *e-mail: eleonora.leucci@kuleuven.be

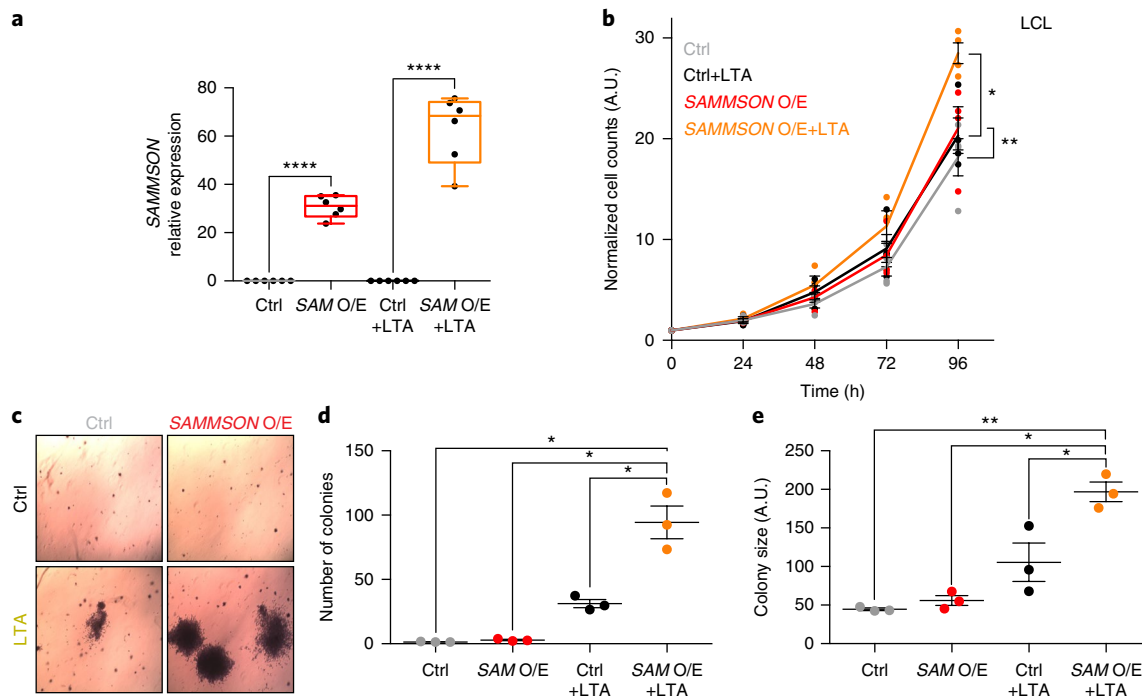


Fig. 1 | SAMMSON induces a malignant phenotype outside of the melanocytic lineage. **a**, SAMMSON expression measured by RT-qPCR in LCL cells infected with an empty (Ctrl) or a SAMMSON-encoding (SAM O/E) expression vector and/or with SV40 LTA; $n = 6$ independent experiments. SAM O/E values are relative to the Ctrl sample and SAM O/E +LTA values are relative to the Ctrl +LTA sample. **b**, Cell proliferation assays in LCL cells described in **a**. Error bars represent mean \pm s.e.m.; $n = 4$ independent experiments. **c**, Soft agar assay in LCL cells described in **a**. Representative images of three independent experiments. **d**, Quantification of number of colonies formed in soft agar as described in **c**. Error bars represent mean \pm s.e.m.; $n = 3$ independent experiments. **e**, Quantification of colony size of soft agar colonies as described in **c**. Error bars represent mean \pm s.e.m.; $n = 3$ independent experiments. P values were calculated by paired two-tailed Student's t -test. * $P < 0.05$; ** $P < 0.01$; **** $P < 0.0001$. A.U.; arbitrary unit. Source data for panels **a**, **b**, **d** and **e** are available in the Supplementary Information.

maturation of mitochondrial rRNAs, is a direct transcriptional target of Myc¹⁸. Attenuation of p32 expression reduces growth rate of glioma cells expressing Myc and impairs tumor formation in vivo¹⁸. Several mitochondrial ribosomal proteins were also identified as Myc targets and, among them, Ptdc3 (pentatricopeptide repeat domain 3) was shown to have a critical role in the maintenance of B-cell lymphomas¹². This data raises the possibility that key oncogenes can directly contribute to the maintenance of the necessary synchronization of the two protein synthesis machineries.

We recently described SAMMSON, a lineage-specific lncRNA aberrantly expressed in a large fraction (>90%) of cutaneous melanoma. Strikingly, melanoma cells are addicted to SAMMSON, irrespective of their genetic make-up or transcriptional state and they quickly undergo apoptosis on its inhibition¹⁹. We showed that SAMMSON interacts with p32 and promotes its efficient targeting to mitochondria¹⁹. Accordingly, SAMMSON depletion caused mitochondrial protein synthesis defects resulting in membrane depolarization and activation of a mPOS-like response¹⁹. It therefore remains unclear whether SAMMSON itself is capable of—concomitantly—provoking an adaptive cytosolic response to ensure a coordinated increase of the cytosolic and mitochondrial translation rates or whether this is driven by SAMMSON-independent mechanisms.

To address this we searched for new SAMMSON-interacting proteins and identified XRN2 (5'-3' Exoribonuclease 2) and CARF (collaborator of ARF, the product of the *CDKN2AIP* gene), two proteins known to play key roles in the biogenesis of cellular ribosomes. XRN2 is a 5'-3' exoribonuclease with a crucial role in the maturation of virtually all RNA species and in nuclear RNA turnover. In the nucleoplasm, XRN2 participates in 3'-end processing of mRNA²⁰ and in the degradation of several transfer RNAs (tRNAs)

including the initiator tRNA(Met) in stress conditions^{21,22}. In the nucleoli, XRN2 is essential for the processing of snoRNA ends^{2,23,24} and for the degradation of spacer fragments that are excised during rRNA maturation, thus ensuring proper maturation of the 5.8S and 28S rRNAs^{2,25}.

XRN2 access to the nucleoli is dynamically regulated by CARF, which titrates XRN2 excess by retaining it in the nucleoplasm to fine-tune pre-rRNA maturation²⁶. Accordingly, CARF overexpression impairs rRNA processing²⁶.

Here we show that SAMMSON promotes CARF binding to p32 thus interfering with its binding to XRN2. This favors XRN2 localization to the nucleoli and p32 targeting to mitochondria and thereby the stimulation of rRNA biogenesis and protein synthesis in both compartments. By boosting translation, SAMMSON confers a growth advantage to immortalized cells irrespective of their tissue of origin.

Results

SAMMSON increases the tumorigenic potential in a lineage-independent fashion. We established that melanoma cells are addicted to SAMMSON independently of their genetic make-up¹⁹. As SAMMSON's expression becomes readily detectable at the early stages of melanomagenesis¹⁹, we asked whether a causative link exists between its expression and malignant transformation. We tested the effects of ectopic SAMMSON expression on immortalized Mel-ST cells belonging to the melanocytic lineage²⁷ (Supplementary Fig. 1). Ectopic expression of SAMMSON under the control of a phosphoglycerate kinase promoter using a lentiviral-based approach, conferred growth advantage in vitro (Supplementary Fig. 1a–d) and allowed tumor growth in nude mice, indicating that its presence

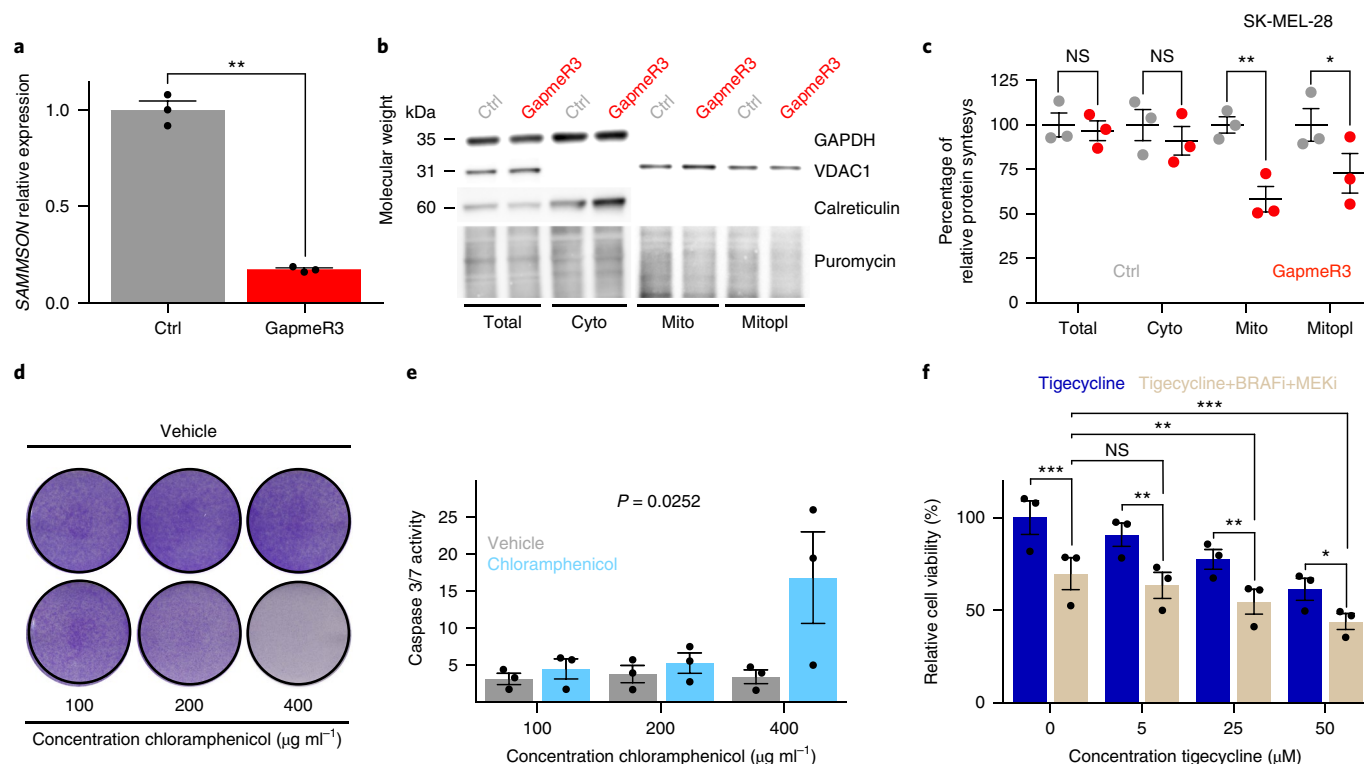


Fig. 2 | Desynchronization of cytosolic and mitochondrial translation machinery decreases melanoma cell fitness and can be therefore exploited therapeutically. **a**, SAMMSON expression measured by RT-qPCR in SK-MEL-28 cells transfected with a non-targeting GapmeR (Ctrl) or GapmeR3. Error bars represent mean \pm s.e.m.; $n=3$ independent experiments. Values are relative to the non-targeting GapmeR (Ctrl) sample. **b**, Western blotting after a 10-min pulse with puromycin and subsequent cytosol (Cyto)-mitochondria (Mito)-mitoplast (Mitopl) fractionation in SK-MEL-28 cells described in **a**. Representative images of three independent experiments. **c**, Quantification of protein synthesis (%), measured by calculating the intensity of the puromycin signal on western blot, in SK-MEL-28 cells as described in **a** and **b**. Error bars represent mean \pm s.e.m.; $n=3$ independent experiments. Values of each cellular fraction are relative to the non-targeting GapmeR (Ctrl) sample. **d**, Colony formation assays 5 days after seeding 1×10^3 SK-MEL-28 cells and treating them with increasing amounts of chloramphenicol or vehicle (EtOH). The violet color is due to crystal violet, a compound that binds intracellular DNA and protein, thus highlighting the cells attached to the plate. Representative image of three independent experiments. **e**, Caspase 3/7 activity 72 h after treating SK-MEL-28 cells with increasing amounts of chloramphenicol or vehicle (EtOH). Error bars represent mean \pm s.e.m.; $n=3$ independent experiments. P values were calculated with two-way ANOVA comparing the two treatments (chloramphenicol versus vehicle). **f**, Cell viability of MM099 cells measured 48 h after treatment with either Tigecycline or a combination of Tigecycline, BRAFi (Dabrafenib) and MEKi (Trametinib). Error bars represent mean \pm s.e.m.; $n=3$ independent experiments. P values were calculated by paired two-tailed Student's t -test. Values are relative to the non-treated sample (first bar on the left). * $P < 0.05$; ** $P < 0.01$; *** $P < 0.001$; NS, not significant. Uncropped gel images are shown in Supplementary Data Set 1. Source data for panels **a**, **c**, **e** and **f** are available in the Supplementary Information.

is sufficient to transform immortalized cells of melanocytic origin (Supplementary Fig. 1e–g).

SAMMSON also conferred a growth advantage to cells that do not belong to the melanocytic lineage, namely the immortalized lymphoblastoid cell line (LCL; SAMMSON-negative) (Fig. 1a,b). Ectopic SAMMSON expression in these cells cooperated with the large T antigen (LTA) in promoting transformation (Fig. 1c–e). The combined expression of SAMMSON and LTA led to an increase in growth that significantly exceeded that of the LTA alone (Fig. 1b). Moreover, while control LCLs were unable to grow in soft agar, LCLs expressing both SAMMSON and LTA were capable of forming more and larger colonies than LCL cells expressing LTA alone (Fig. 1c–e). These findings demonstrated the ability of SAMMSON to enhance malignant transformation within and outside the melanocytic lineage.

Desynchronization of cytosolic and mitochondrial translation machinery is detrimental and can be exploited therapeutically. We established that knockdown of SAMMSON decreases melanoma viability by impairing mitochondrial translation and inducing an mPOS-like response¹⁹. This finding suggested that

disruption of the equilibrium between cytosolic and mitochondrial protein synthesis impairs melanoma cell fitness¹³. Accordingly, acute depletion of SAMMSON using antisense oligonucleotides¹⁹ in the established melanoma line SK-MEL-28 (Fig. 2a) caused severe defects in mitochondrial protein synthesis (Fig. 2b,c) and apoptotic responses¹⁹ before any impact on cytosolic protein synthesis could be observed (Fig. 2b,c). Both antisense oligonucleotides (GapmeR3 and 11) have previously been selected for their ability to efficiently decrease SAMMSON expression without causing any off-target effects¹⁹.

Loss of cell viability induced by SAMMSON knockdown was phenocopied by specific inhibition of mitochondria protein synthesis using chloramphenicol (Fig. 2d,e). Designed to target bacterial ribosomes, chloramphenicol and antibiotics of the tetracyclines family are also effective in inhibiting the structurally related mitribosomes^{11,12}. Consequently, survival of SK-MEL-28 melanoma cells exposed to chloramphenicol was compromised in a dose-dependent manner (Fig. 2d,e). This data identified the balance between cytosolic and mitochondrial protein synthesis rates as an exploitable therapeutic vulnerability in melanoma. Accordingly, an antibiotic in clinical use such as Tigecycline sensitized ‘invasive’ therapy

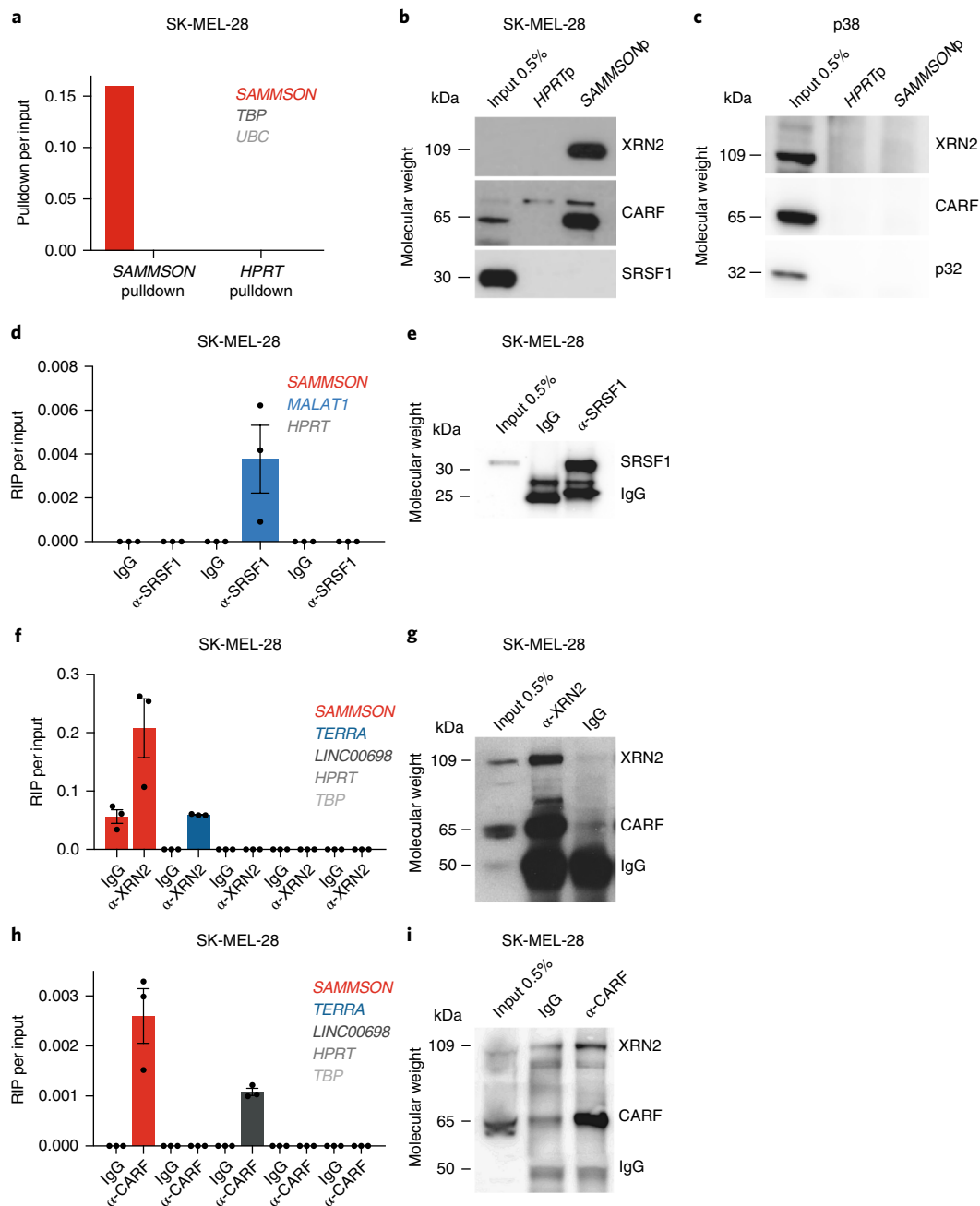


Fig. 3 | SAMMSON interacts with XRN2 and CARF. **a**, SAMMSON (but not TBP or UBC) is specifically recovered by RNA antisense purification (RAP) after ultraviolet crosslinking SK-MEL-28 cells as measured by RT-qPCR. Enrichments were calculated by normalizing the RAP over the inputs using the $\Delta \Delta C_i$ method (see Methods). Genes not detectable in the RAP were assigned a value of 0. Representative graph of three independent experiments. **b**, SAMMSON and HPRT pulldown in native conditions (using two sets of 48 biotinylated probes recognizing mature transcripts, *p*) and western blotting with anti-XRN2, anti-CARF and anti-SRSF1 antibodies in SK-MEL-28 cells. Representative image of three independent experiments. **c**, SAMMSON and HPRT pulldown in native conditions (using biotinylated probes, *p*) and western blotting in mouse p38 cells with anti-XRN2, anti-CARF and anti-p32 antibodies. Representative image of three independent experiments. **d**, MALAT1 (but not SAMMSON or HPRT) is recovered by RNA immunoprecipitation (RIP) using an SRSF1-specific antibody as measured by RT-qPCR in SK-MEL-28 cells. Enrichments were calculated by normalizing the RIP over the inputs using the $\Delta \Delta C_i$ method (see the Methods section). Genes not detectable in the RIP were assigned a value of 0. Error bars represent mean \pm s.e.m.; *n* = 3 independent experiments. **e**, Western blot with an anti-SRSF1 antibody following RIP with an anti-SRSF1 antibody in SK-MEL-28 cells. Representative image of three independent experiments. **f**, SAMMSON and TERRA are recovered by RIP using an XRN2-specific antibody as measured by RT-qPCR in SK-MEL-28 cells. Enrichments were calculated by normalizing the RIP over the inputs using the $\Delta \Delta C_i$ method (see Methods). Genes not detectable in the RIP were assigned a value of 0. Error bars represent mean \pm s.e.m.; *n* = 3 independent experiments. **g**, Western blot with anti-XRN2 and anti-CARF antibodies following RIP with an anti-XRN2 antibody in SK-MEL-28 cells. Representative image of three independent experiments. **h**, SAMMSON and LINC00698 are recovered by RIP using a CARF-specific antibody as measured by RT-qPCR in SK-MEL-28 cells. Enrichments were calculated by normalizing the RIP over the inputs using the $\Delta \Delta C_i$ method (see the Methods section). Genes not detectable in the RIP were assigned a value of 0. Error bars represent mean \pm s.e.m.; *n* = 3 independent experiments. **i**, Western blot with anti-XRN2 and anti-CARF antibodies following RIP with an anti-CARF antibody in SK-MEL-28 cells. Representative image of three independent experiments. Uncropped gel images are shown in Supplementary Data Set 1. Source data for panels **a**, **d**, **f** and **h** are available in the Supplementary Information.

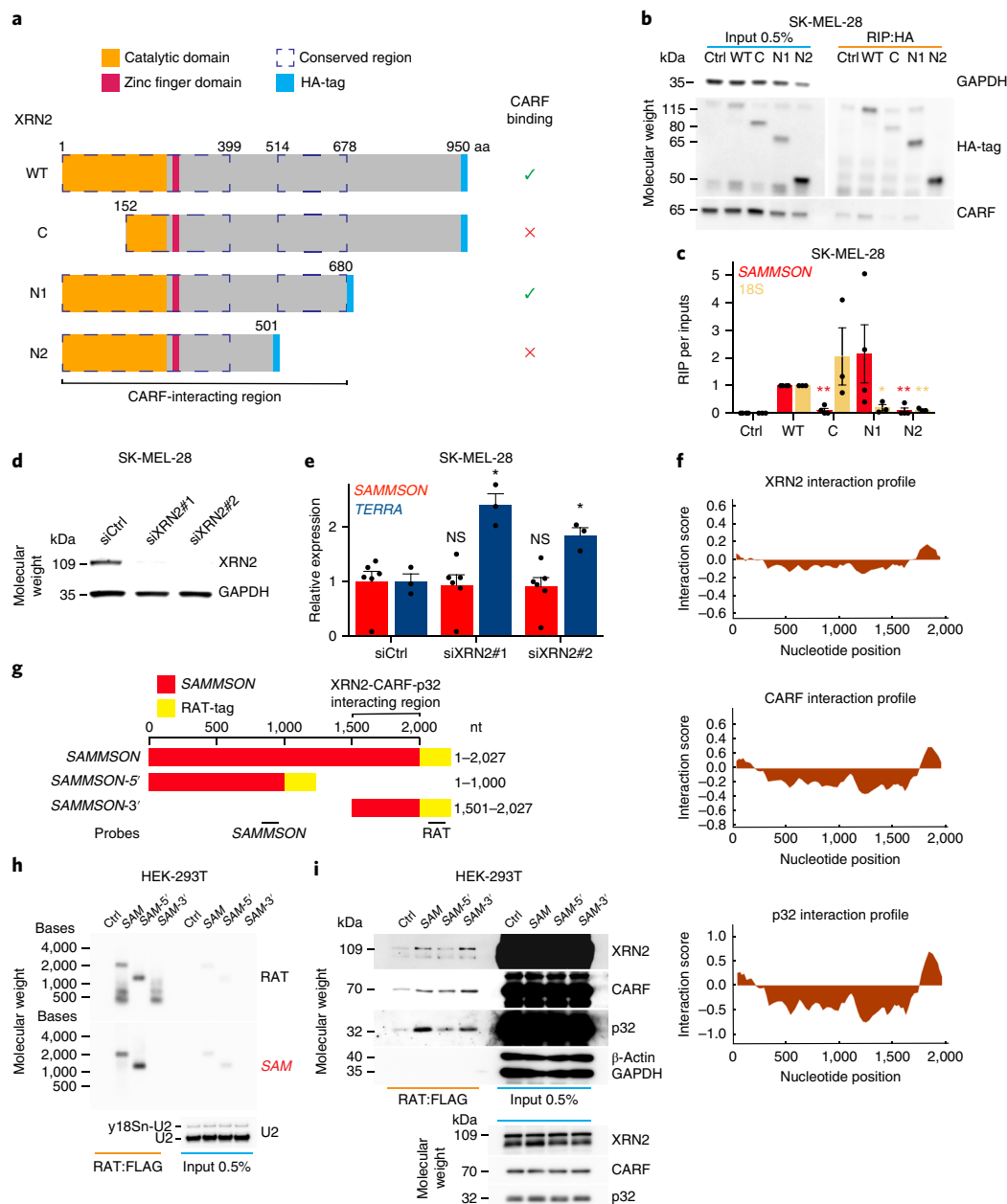


Fig. 4 | Identification of SAMMSON-binding region on XRN2 and of SAMMSON protein-binding domain. **a**, Schematic representation of the different HA-XRN2-constructs. **b**, Western blot with anti-HA-tag (top) and anti-CARF (bottom) antibodies in SK-MEL-28 cells transfected with different HA-tagged XRN2 constructs or an untransfected control (Ctrl) followed by RIP with an anti-HA-tag antibody. Representative images of four independent experiments. **c**, SAMMSON and 18S are recovered by RIP using a HA-tag-specific antibody only in one out of the three XRN2 deletion constructs (N1 and C, respectively) as measured by RT-qPCR in SK-MEL-28 cells. All deletion mutants were normalized on the positive control (WT) sample. Red asterisks refer to the statistical significance of SAMMSON retrieval after RIP, calculated using a paired two-tailed Student's *t*-test comparing the WT XRN2 construct versus the three different XRN2 deletion constructs. Yellow asterisks refer to the statistical significance of 18S retrieval after RIP, calculated using a paired two-tailed Student's *t*-test comparing the WT XRN2 construct versus the three different XRN2 deletion constructs. Error bars represent mean \pm s.e.m.; SAMMSON, *n* = 4 independent experiments; 18S, *n* = 3 independent experiments. **d**, Western blotting of XRN2 in SK-MEL-28 cell lysates 72 h after transfection with a control siRNA (siCtrl) or two different siRNAs targeting XRN2. Representative images of six independent experiments. **e**, SAMMSON and TERRA expression as measured by RT-qPCR in SK-MEL-28 cells treated as described in **d**. Values are relative to the siRNA control (siCtrl) sample and were normalized independently for SAMMSON and TERRA. Error bars represent mean \pm s.e.m.; SAMMSON, *n* = 6 independent experiments; TERRA, *n* = 3 independent experiments. **f**, Binding of SAMMSON to XRN2, CARF and p32 were predicted using the *catRAPID*^{54,55}. Background correction was obtained by subtracting the profile of aquaporin 1 (AQP1), a bona fide negative control not retrieved in the mass spectrometry data from SAMMSON pull-down. **g**, Schematic representation of the different SAMMSON_RAT-tag constructs, **h**, FLAG-tag RIP in HEK-293T cells transfected either with the different SAMMSON constructs or control plasmid (Ctrl) followed by northern blot using the probes for the RAT-tag and SAMMSON indicated in **g**. Representative images of three independent experiments. **i**, Western blot with the protein fraction recovered from the RIP experiment described in **h**. Top panel long exposure, bottom panel short exposure (for Input 0.5% only). Representative images of three independent experiments. *P* values were calculated by paired two-tailed Student's *t*-test. **P* < 0.05; ***P* < 0.01; NS, not significant. Uncropped gel images are shown in Supplementary Data Set 1. Source data for panels **c** and **e** are available in the Supplementary Information.

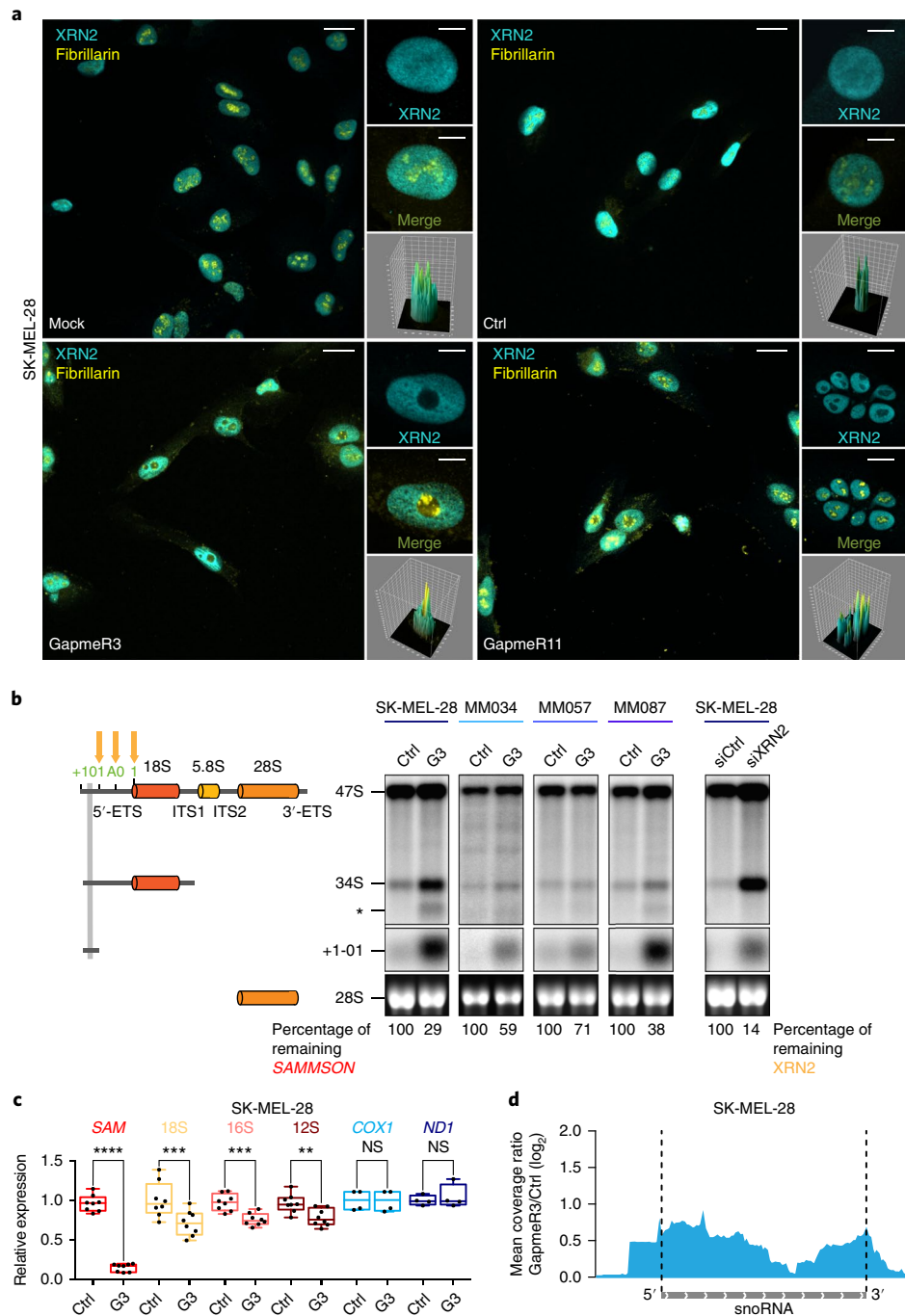


Fig. 5 | SAMMSON modulates XRN2 localization and function. **a**, Representative XRN2 (cyan) and fibrillarin (yellow) immunofluorescence (IF) in SK-MEL-28 cells 30 h after transfection with a non-targeting GapmeR (Ctrl), GapmeR3 or GapmeR11 or without transfection (Mock). Scale bar low magnification, 10 μ m; high magnification, 2 μ m. Representative images of three independent experiments. **b**, Left, schematic representation of the pre-rRNAs and the mature rRNAs detected by northern blotting, orange arrows indicate the sites of pre-rRNA-processing inhibition in the 5'-ETS (O1, A0 and 1). The probe used for northern blotting is highlighted in grey. ETS: external transcribed spacers; ITS: internal transcribed spacers. The aberrant 34S RNA is produced when cleavage occurs in ITS1 prior to 5'-ETS. *, truncated form of the 34S RNA. Right, northern blot hybridization analysis of pre-rRNA isolated from four melanoma cell lines (with different mutational backgrounds and phenotype) transfected with a non-targeting GapmeR (Ctrl), GapmeR3 (G3) or of SK-MEL-28 transfected with a XRN2-targeting (siXRN2) or control (siCtrl) siRNA. Knock-down efficiency is indicated for both SAMMSON knockdown and XRN2 knockdown below the blot. Representative image of three independent experiments. **c**, SAMMSON (SAM), 18S, 16S, 12S, Cyclooxygenase 1 (COX1) and NADH-ubiquinone oxidoreductase chain 1 (ND1) expression measured by RT-qPCR in SK-MEL-28 cells 30 h after transfection with a non-targeting GapmeR (Ctrl) or with GapmeR3 (G3); $n = 8$ independent experiments for SAMMSON, 18S, 16S and 12S; $n = 4$ independent experiments for COX1 and ND1. Values are relative to the non-targeting GapmeR (Ctrl) sample. **d**, Mean coverage ratio between SAMMSON knockdown and a non-targeting GapmeR across all expressed snoRNAs. Data are displayed for a snoRNA meta-gene, demonstrating increased coverage beyond the snoRNA boundaries. Box boundaries represent 25th and 75th percentiles; center line represents the median; whiskers, last data point within a ± 1.5 interquartile range. P values were calculated by paired two-tailed Student's t -test. ** $P < 0.01$; *** $P < 0.001$; **** $P < 0.0001$; NS, not significant. Uncropped gel images are shown in Supplementary Data Set 1. Source data for panel **c** are available in the Supplementary Information.

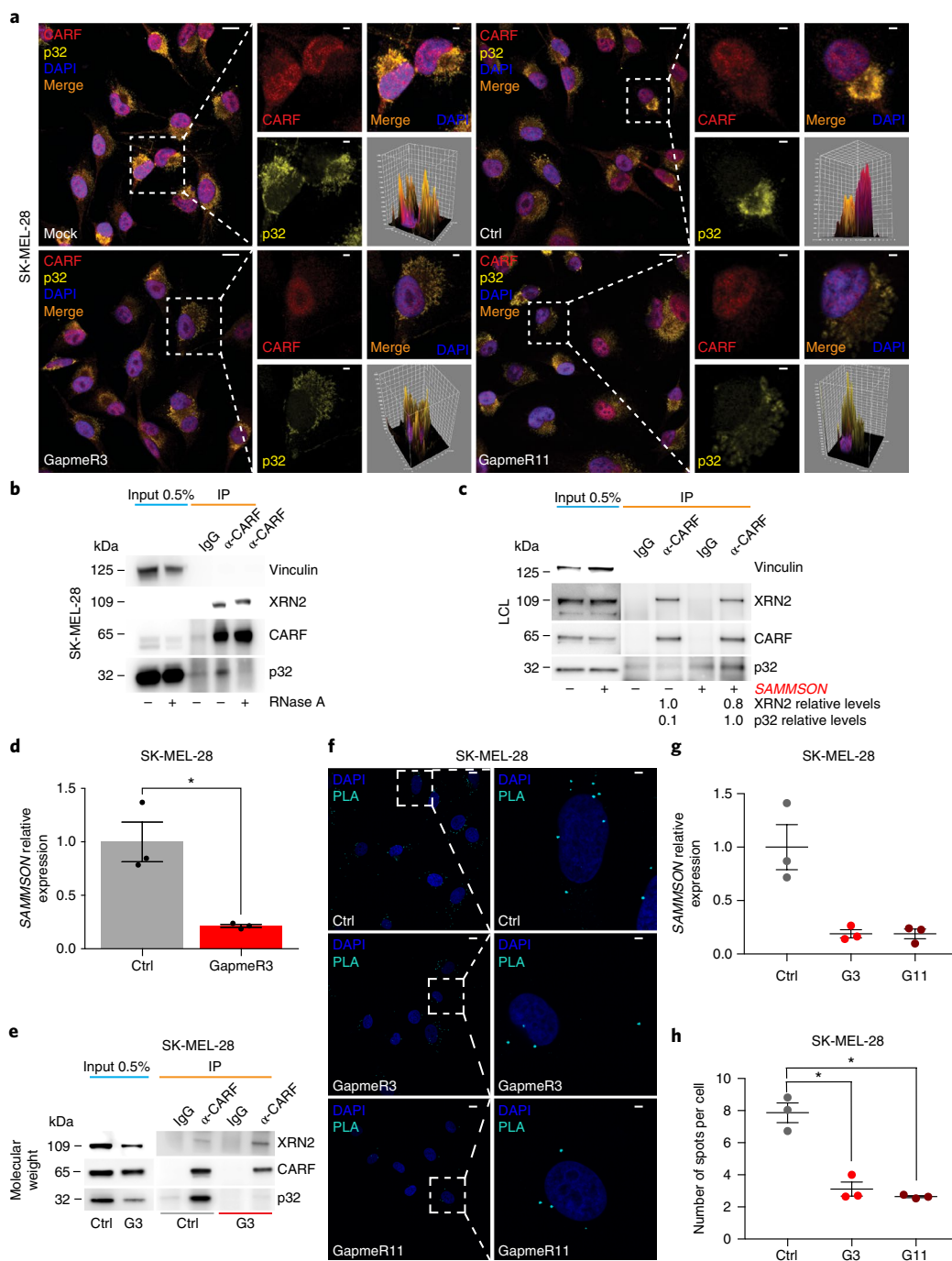


Fig. 6 | SAMMSON promotes CARF localization to the cytoplasm and its binding to p32. **a**, CARF (red) and p32 (yellow) IF in SK-MEL-28 cells 30 h after transfection with a non-targeting GapmeR (Ctrl), GapmeR3 or GapmeR11 or untransfected (Mock). Cell nuclei are stained with DAPI (blue). Scale bar low magnification, 10 μ m; high magnification, 2 μ m. Representative images of three independent experiments. **b**, CARF immunoprecipitation (IP) in SK-MEL-28 cells in the presence (+) or absence (–) of RNase A, followed by western blotting with the indicated antibodies. Representative image of three independent experiments. **c**, CARF IP in LCL cells described in Fig. 1a, followed by western blotting with the indicated anti-bodies. (–) represents cells infected with an empty control plasmid and (+) cells infected with a SAMMSON-encoding plasmid. Representative image of three independent experiments. **d**, SAMMSON expression measured by RT-qPCR in SK-MEL-28 cells 30 h after transfection with a non-targeting GapmeR (Ctrl) or GapmeR3 (G3). Error bars represent mean \pm s.e.m.; $n = 3$ independent experiments. Values are relative to the non-targeting GapmeR (Ctrl) sample. **e**, CARF IP in SK-MEL-28 cells treated as described in **d**, followed by western blotting with the indicated antibodies. Representative images of three independent experiments. **f**, PLA (cyan) assay using antibodies against CARF and p32 in SK-MEL-28 cells 30 h after transfection with a non-targeting (Ctrl), GapmeR3 or GapmeR11. Cell nuclei are stained with DAPI (blue). Scale bar low magnification, 10 μ m; high magnification, 2 μ m. Representative images of three independent experiments. **g**, SAMMSON expression measured by RT-qPCR in SK-MEL-28 cells 30 h after transfection with a non-targeting GapmeR (Ctrl), GapmeR3 (G3) or GapmeR11 (G11). Error bars represent mean \pm s.e.m.; $n = 3$ independent experiments. Values are relative to the non-targeting GapmeR (Ctrl) sample. **h**, Quantification of PLA assay described in **f**. Error bars represent mean \pm s.e.m.; $n = 3$ independent experiments. P values were calculated by paired two-tailed Student's t -test. * $P < 0.05$. Uncropped gel images are shown in Supplementary Data Set 1. Source data for panels **d**, **g** and **h** are available in the Supplementary Information.

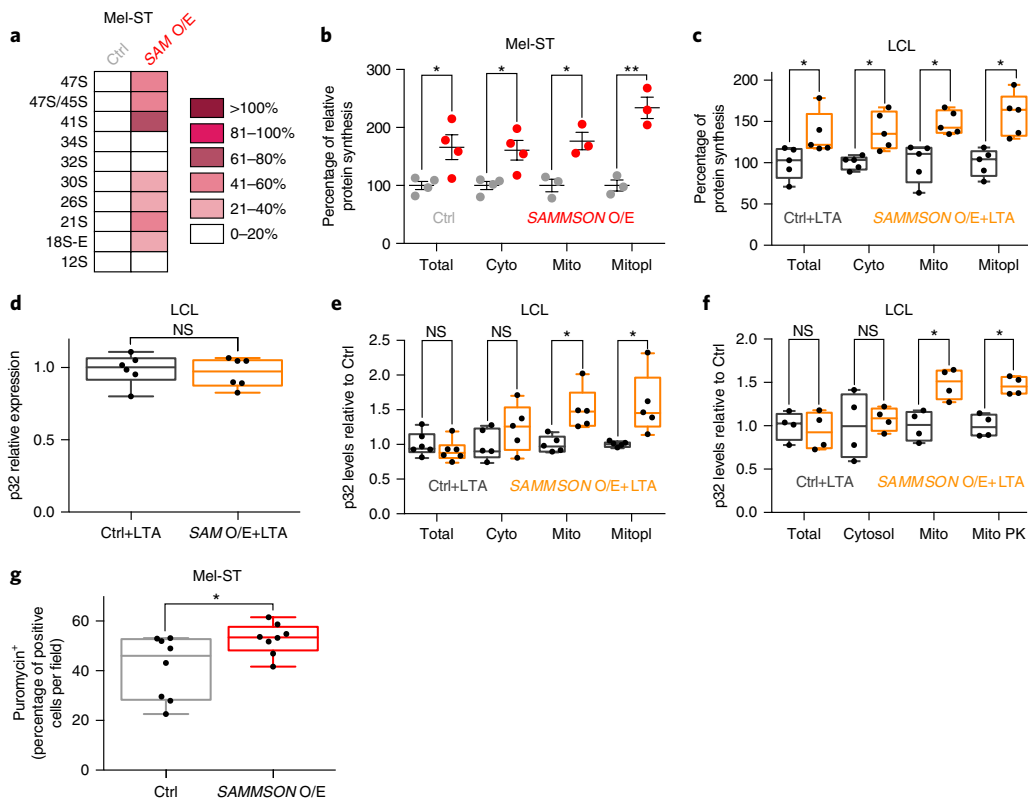


Fig. 7 | SAMMSON expression increases rRNA processing thus promoting protein synthesis. **a**, Heatmap representation of pre-rRNA analysis in Mel-ST cells overexpressing SAMMSON (SAM O/E) relative to cells transfected with an empty (Ctrl). Each pre-rRNA intermediate detected was quantified with a PhosphorImager; $n = 3$ independent experiments. **b–c**, Quantification of relative protein synthesis (%), measured by calculating the intensity of the puromycin signal on western blot, after a 10-min pulse with puromycin and subsequent cytosol (Cyto)-mitochondria (Mito)-mitoplast (Mitopl) fractionation followed by western blot in Mel-ST cells described in **a**, **b**, or LCL cells infected with the SV40 Large T Antigen and with an empty (Ctrl + LTA) or a SAMMSON-encoding (SAMMSON O/E + LTA) expression vector (**c**). Error bars represent mean \pm s.e.m. Total and Cyto, $n = 4$ independent experiments; Mito and Mitopl, $n = 3$ independent experiments for Mel-ST cells, $n = 5$ independent experiments for LCL cells. Values of each cellular fraction are relative to the Ctrl sample (**b**) or to the Ctrl + LTA sample (**c**). **d**, p32 expression measured by RT-qPCR in LCL cells as described in **c**; $n = 6$ independent experiments. Values are relative to the Ctrl + LTA sample. **e**, Quantification of p32 protein levels in LCL cells described in **c** after cytosol (Cyto)-mitochondria (Mito)-mitoplast (Mitopl) fractionation; $n = 6$ independent experiments. Values of each cellular fraction are relative to the Ctrl + LTA sample. **f**, Quantification of p32 protein levels after cytosol (Cyto)-mitochondria (Mito)-protease K-treated mitochondria (Mito + PK) fractionation in LCL cells as described in **c**; $n = 4$ independent experiments. Values of each cellular fraction are relative to the Ctrl + LTA sample. **g**, Puromycin quantification (each point represents the average of the quantification of three different fields) of tumors as described in Supplementary Fig. 1e–g; $n = 8$ independent experiments. For box blots, box boundaries represent 25th and 75th percentiles; center line represents the median; whiskers, last data point within a ± 1.5 interquartile range. P values were calculated by paired two-tailed Student's t -test. * $P < 0.05$; ** $P < 0.01$; NS, not significant. Source data for panels **b–g** are available in the Supplementary Information.

resistant)²⁸ melanoma cells (MM099) to the combination of Dabrafenib and Trametinib (Fig. 2f).

This data demonstrated the importance of a coordinated translation in both compartments and indicated that disruption of mitochondrial translation is a valuable antimelanoma strategy.

SAMMSON interacts with CARF and XRN2, two proteins involved in ribosome biogenesis. Given that expression of SAMMSON is sufficient to promote malignant transformation and that cancer cell fitness depends on a synchronized increase in protein translation in the mitochondria and cytosol we hypothesized that SAMMSON may also control cytosolic translation. A search in our list of putative SAMMSON's interacting partners¹⁹ identified XRN2 and CARF, two proteins implicated in ribosome biogenesis in the nucleus. Both proteins showed elevated expression in melanoma compared to normal human epidermal melanocytes (NHEM; Supplementary Fig. 2a). We confirmed the ability of SAMMSON to interact with these proteins using RNA pull-downs and RNA immunoprecipitations (RIP). By specifically pulling-down SAMMSON using a pool of

antisense oligonucleotides in native (Fig. 3a,b) and crosslinking conditions (Supplementary Fig. 2b), we observed a robust enrichment for CARF and XRN2 (Fig. 3b and Supplementary Fig. 2b). In contrast, other abundant proteins such as vinculin or the RNA-binding protein SFRS1 could not be detected (Fig. 3b and Supplementary Fig. 2b). Additionally, no enrichment for these proteins was observed when performing the assay in the SAMMSON-negative mouse cell line p38 (Fig. 3c). Conversely, the lincRNA MALAT1 an established SFRS1-partner²⁹, but not SAMMSON, was identified in SFRS1-immunoprecipitates (Fig. 3d,e). Likewise, RNA fractions obtained from XRN2 and CARF immunoprecipitates (Fig. 3g,i) were enriched in SAMMSON, but not in the cytosolic RNAs *TBP* and *HPRT* (Fig. 3f–h). Further confirming the interaction, *TERRA*, a known XRN2 substrate³⁰, was retrieved in XRN2, but not in CARF immunoprecipitates. In contrast, CARF, but not XRN2, associated specifically with another melanoma-specific lincRNA (*LINC00698*). This data validated CARF and XRN2 as bona fide SAMMSON interactors.

Consistent with previous findings, CARF and XRN2 co-immunoprecipitated (Fig. 3g,i) confirming their physical interaction²¹.

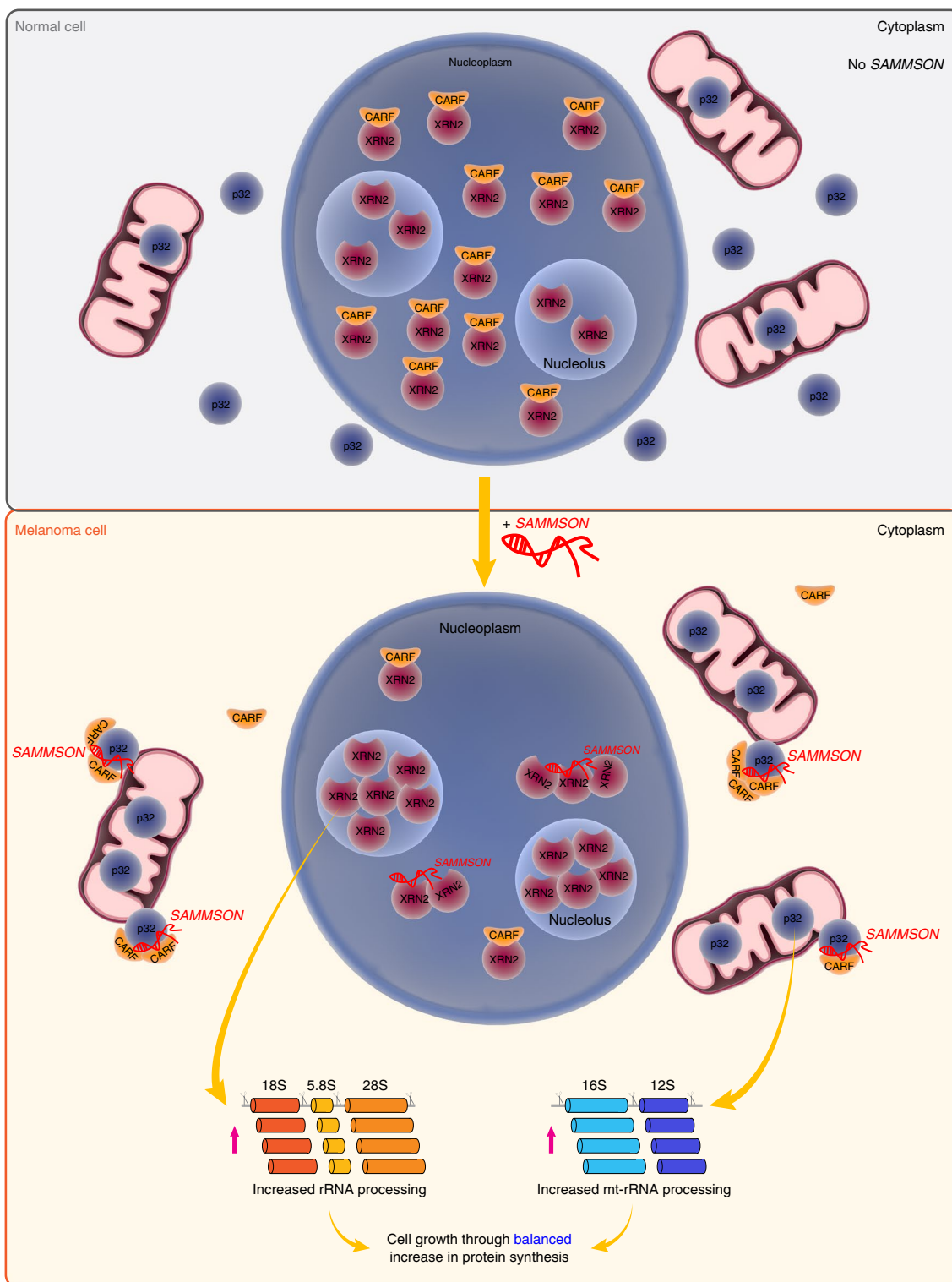


Fig. 8 | Schematic representation of SAMMSON mechanism of action. In normal (SAMMSON-negative) cells, CARF controls the nuclear localization of XRN2 by sequestering a pool of XRN2 in the nucleoplasm. In the context of melanoma, SAMMSON expression promotes the interaction of CARF with p32 in the cytoplasm at the expense of the CARF-XRN2 interaction, thus favoring p32 mitochondrial localization and XRN2 nucleolar localization. By modulating these interactions SAMMSON determines a balanced increase in rRNA maturation and protein synthesis in the cytosol and mitochondria. As a result, SAMMSON promotes cell growth.

This observation raised the possibility that SAMMSON may be engaged into a ribonucleoprotein complex containing both XRN2 and CARF. Alternatively, SAMMSON may interact with both

proteins independently, and even possibly modulate the XRN2-CARF association. To address this, we mapped the XRN2-SAMMSON's interaction interface using three different HA-tagged

XRN2-deletion constructs²⁶ (Fig. 4a). An interaction between *SAMMSON* and wild-type XRN2 was readily detected by RIP assays (Fig. 4b,c). Although *SAMMSON* did interact with the N1 form of XRN2, which lacks the last 270 amino acids, further deletion of another 171 amino acids containing an evolutionarily conserved region (mutant N2), abrogated the binding. Interestingly, this conserved domain was also required for the interaction between XRN2 and CARF (Fig. 4b,c)²⁸.

Similarly to CARF, *SAMMSON* was also incapable of binding a XRN2 mutant lacking the first 152 amino acids (mutant C), which constitutes a large part of the catalytic domain. In contrast, the 18S ncRNA, known to be a XRN2 substrate²⁵, required an intact carboxy-terminal half of the protein for binding, and did not occupy the catalytic domain (Fig. 4c). These observations could indicate that *SAMMSON* may modulate XRN2 functions rather than being a direct XRN2 substrate. In keeping with this, silencing XRN2 stabilized *TERRA*, a known XRN2 substrate, but did not affect *SAMMSON* levels (Fig. 4d,e).

To identify which portion of *SAMMSON* is responsible for binding to XRN2, CARF and p32, we predicted their interactions *ab initio* using *catRAPID*³¹. *catRAPID* predicted an interaction interface with all three proteins located in a region comprising the last 400–300 nucleotides of *SAMMSON* (Fig. 4f). Based on these findings, we designed two *SAMMSON* deletion mutants, in which we also inserted a RAT (RNA affinity in tandem)-tag (Fig. 4g). The aptamer recognizing the RAT-tag was FLAG-conjugated thus allowing us to purify *SAMMSON*-containing complexes with an anti-FLAG antibody. The experiment (Fig. 4h) confirmed the *in silico* predictions, since deletion of the last 500 nucleotides of the *SAMMSON* sequence impaired its ability to interact with XRN2, CARF and p32 (Fig. 4i). These data indicated that the 3'-end of *SAMMSON* engages in multiple protein interactions.

***SAMMSON* modulates XRN2 localization and nucleolar functions.** CARF regulates XRN2 access to the nucleoli (and related functions) by tethering it into the nucleoplasm²⁶. To further investigate the relationship between XRN2, CARF and *SAMMSON*, we determined the localization of CARF and XRN2 on *SAMMSON* knockdown. Immunofluorescent staining revealed that *SAMMSON* silencing led to the complete exclusion of XRN2 from the nucleoli (Fig. 5a) and relocation of the cytoplasmic fraction of CARF to the nucleoplasm (Supplementary Fig. 3a).

To rule out the possibility that the nucleoplasmic relocation of XRN2 was an indirect consequence of the mitochondrial stress triggered by *SAMMSON* knockdown¹⁹, we interfered with mitochondrial translation via a distinct mechanism³² by treating the cells with chloramphenicol and determined XRN2 localization (Supplementary Fig. 3b,c). This confirmed that XRN2 localization was not affected by this treatment (Supplementary Fig. 3b,c). Moreover, XRN2 localization was also unaffected by the silencing of *NEAT1*, another lncRNA reported to interact with XRN2³³ and implicated in stress responses³⁴ (Supplementary Fig. 3d,e). Hence, the displacement of XRN2 from the nucleoli is a direct consequence of *SAMMSON*'s silencing.

XRN2 modulates the biogenesis of the cytosolic ribosome by processing the rRNA and snoRNA in the nucleolus. Displacement of XRN2 away from the nucleoli in *SAMMSON*-depleted cells indicated that *SAMMSON* is likely to modulate XRN2 nucleolar functions. Similar to XRN2 knockdown, *SAMMSON* knockdown caused the accumulation of an aberrant precursor, the 34S pre-rRNA, which arises from the inhibition in the cleavage of the 5'-ETS (external transcribed spacer; Fig. 5b and Supplementary Fig. 4a). Processing in the 5'-ETS and turnover of the cleaved fragments are intimately connected³⁵. Accordingly, inhibition of the cleavage increased the amount of the fragment +1-01 (Fig. 5b and Supplementary Fig. 4a). As a consequence, we observed an imbalanced production of 18S

(Fig. 5c and Supplementary Fig. 4b). Moreover, consistent with previous data showing impaired mitochondrial targeting of p32 and defective mitochondrial rRNA processing¹⁹, levels of mitochondrial rRNAs (12S and 16S) were also decreased (Fig. 5c and Supplementary Fig. 4b) while the expression of mitochondrial rRNA precursors slightly increased as a result of the defective processing (Supplementary Fig. 4c). Conversely, other mitochondrial transcripts remained unaffected (Fig. 5c and Supplementary Fig. 4b).

Nucleolar XRN2 is also implicated in the maturation of the 5'-ends of snoRNAs^{2,23,24}. SnoRNAs are largely encoded in host gene introns and produced by endo- and exoribonucleolytic digestion of spliced-lariats^{36,37}. Consistently, we detected aberrant 5' extended forms of snoRNA precursors on *SAMMSON* silencing (Fig. 5d). Note that the processing of the 3'-end of snoRNA precursors was also affected. This may indicate that XRN2-mediated 5'-end processing is required for subsequent trimming of the 3'-end.

In addition to its nucleolar functions XRN2 also exhibits a nucleoplasmic function linked to translation, such as the processing and degradation of initiator tRNAMet²¹. Consistent with the complete re-localization of XRN2 into the nucleoplasm, a decreased expression of the initiator tRNA for methionine (tRNA^{Met}) was observed on *SAMMSON* depletion (Supplementary Fig. 4d). This data indicated that *SAMMSON* favors XRN2 localization to nucleoli and promotes its ability to support ribosome biogenesis.

***SAMMSON* rewires the melanoma RNA-binding protein network involved in ribosome biogenesis.** XRN2 exclusion from the nucleoli and its increased co-localization with CARF in the nucleoplasm on *SAMMSON* knockdown indicated that *SAMMSON* may interfere with CARF binding to XRN2. However, while *SAMMSON* is predominantly cytoplasmic¹⁹, XRN2 is exclusively nuclear. CARF instead, has been detected in both the nucleoplasm, where the interaction with XRN2 takes place²⁶, and the cytoplasm, where its function remains unclear (Fig. 6a). Consistently, a pool of CARF was detected in the cytoplasm of melanoma cells (Fig. 6a). Immunostaining for CARF and p32, another validated *SAMMSON*'s interacting partner¹⁹, indicated that the two proteins co-localized in the cytoplasm of melanoma cells and their co-localization was lost on silencing of *SAMMSON*, when CARF relocated to the nucleus (Fig. 6a). Consistent with our findings showing that *SAMMSON* promotes mitochondrial targeting of p32¹⁹, *SAMMSON*'s depletion also affected the localization of p32 that diffusely localized to the cytoplasm and partly to the nucleus in *SAMMSON* knockdown cells (Supplementary Fig. 5a).

We then investigated the possibility that *SAMMSON*, CARF and p32 are engaged into a ribonucleoprotein complex. We performed RIP using melanoma cell extracts supplemented with RNase A (Fig. 6b). While p32 was readily detectable in CARF immunoprecipitates in absence of RNase A treatment, this interaction was abrogated in the presence of RNase A (Fig. 6b). Similar results were obtained with proximity ligation assay (PLA) for CARF and p32 (Supplementary Fig. 5b). Conversely, similar RIP experiments in LCLs, which do not express *SAMMSON*, failed to detect an association between CARF and p32 (Fig. 6c and Supplementary Fig. 5c). This data indicated that p32 and CARF interact specifically in melanoma cells and in an RNA-dependent manner. To test whether this interaction is mediated by *SAMMSON* itself, we used LCLs and assessed binding between CARF and p32 using RIP assays (Fig. 6c and Supplementary Fig. 5c, respectively). Ectopic expression of *SAMMSON* alone was sufficient to trigger the binding between CARF and p32 and promoted export of a fraction of CARF to the cytoplasm (Supplementary Fig. 5d). Accordingly, knockdown of CARF affected the mitochondrial network architecture (Supplementary Fig. 6a).

Moreover, PLA in Mel-ST expressing *SAMMSON* ectopically further confirmed that the interaction is *SAMMSON*-dependent (Supplementary Fig. 6b).

Conversely, RIP for CARF showed increased binding of XRN2 to CARF in *SAMMSON* knockdown cells and this occurred at the expense of CARF-p32 interaction (Fig. 6d,e and Supplementary Fig. 6c,d). PLA further confirmed that *SAMMSON* silencing decreases the number of interactions between CARF and p32 (Fig. 6f–h).

These findings established that *SAMMSON*'s expression is sufficient to trigger an 'aberrant' interaction between CARF and p32 to promote CARF re-localization to the cytoplasm. Remarkably, ectopic expression of *SAMMSON* was sufficient to drive this interaction even in cells that are not derived from the melanocytic lineage.

***SAMMSON* promotes translation in both the cytosol and mitochondria.** This data indicated that *SAMMSON* may stimulate ribosome biogenesis to concertedly increase mitochondrial and cytosolic translation. Consistently, ectopic expression of *SAMMSON* in the immortalized human Mel-ST cells resulted in an increased amount of nuclear rRNA (Fig. 7a and Supplementary Fig. 7a). *SAMMSON* expression also resulted in global increase in de novo translation rates in both cytosolic and mitochondrial compartments, as illustrated by puromycin incorporation assay (SUnSET³⁸) (Fig. 7b and Supplementary Fig. 7b). Importantly, the increase in translation was detectable 30 h after transfection, before any significant impact on cell proliferation could be measured (48 h time point; Fig. 1b and Supplementary Fig. 1b). This observation rules out the possibility that the increase in translation rate is a consequence of increased cell proliferation. Increased translation was also detected in Mel-ST xenografts (Fig. 7g and Supplementary Fig. 7f,g). Similar results were obtained in the LCLs transduced with *SAMMSON* and the LTA (Fig. 1). Overexpression of *SAMMSON*, but not LTA alone, induced a robust increase in translation in both compartments (Fig. 7c and Supplementary Fig. 7c). This result was further confirmed by metabolic labeling with L-azidohomoalanine followed by extraction of mitochondria in proteinase K on *SAMMSON* overexpression, thus indicating that the increased signal was unlikely to derive from cytosolic ribosomes attached to the mitochondrial membrane (Supplementary Fig. 7e). Consistent with previous results¹⁹, we could not detect any change in p32 mRNA expression (Fig. 7d), however, its protein levels in the mitochondria were significantly increased (Fig. 7e,f and Supplementary Fig. 7c,d). We concluded that *SAMMSON* is capable of stimulating ribosome biogenesis, and thereby protein synthesis, by rewiring complex formation and cellular localization of proteins involved in the maturation of nuclear and mitochondrial rRNA.

Discussion

Nucleolar hypertrophy has long been recognized as a hallmark of cancer³⁹ and changes in nucleolar functions contributes to malignant transformation. Accordingly, several RNA polymerase I inhibitors have been introduced in the clinic and/or enrolled into clinical trials^{40,41}. A growing body of evidence indicates that quantitative and qualitative reprogramming of cytosolic and mitochondrial translation are required to sustain tumor development and progression⁴². Moreover, cytosolic and mitochondrial protein synthesis machineries need to be balanced to avoid proteotoxic stress^{4,43,44}. While mitochondria are relatively efficient at adjusting their protein synthesis rate to the income in cytosolic proteins⁴⁴, deregulation of mitochondrial translation invariably induces detrimental responses^{19,45}, probably due to the higher stability of cytosolic ribosomes and to the multiple regulatory steps downstream of ribosome biogenesis. Our data suggests that disruption of this equilibrium by blocking mitochondrial translation, either by knocking down lineage-specific lncRNAs, such as *SAMMSON* or treatment with antibiotics, can be exploited therapeutically to kill cancer cells.

We previously showed that melanoma cells are addicted to *SAMMSON*, a lncRNA interacting with p32 to regulate mitochondrial

protein synthesis¹⁹. Here, we establish *SAMMSON* as a key player in nuclear-mitochondrial communication and a guardian of proteostasis in melanoma. It stimulates rRNA maturation in the nucleoli and increases the rate of cytosolic protein synthesis (Fig. 8).

SAMMSON participates in the reprogramming of the nucleolar activities in this context by modulating the subcellular localization of XRN2 (Fig. 8). Through this process, *SAMMSON* stimulates rRNA and snoRNA processing in the nucleoli, stabilizes tRNA^{Met} in the nucleoplasm and, ultimately, increases translation in the cytosol, thus increasing cancer cell fitness.

The ability of *SAMMSON* to perturb the formation of a complex between CARF and XRN2 was unexpected considering that the CARF-XRN2 interaction was reported to be RNA-independent²⁶.

Our data indicates that *SAMMSON* may interfere with the formation of the CARF-XRN2 complex via distinct mechanisms and the relative contributions of these mechanisms remains to be established.

Since both *SAMMSON* and CARF bind to overlapping domains of XRN2, *SAMMSON* may either mask the CARF binding site or promote (or impair) the deposition of post-translational modifications that affects XRN2 localization and (or) function. In addition, in presence of *SAMMSON*, CARF switches from a nuclear complex with XRN2 to an aberrant complex with p32 into the cytoplasm. CARF cytoplasmic re-localization physically limits its ability to interact with XRN2, which is exclusively nuclear. XRN2 exerts specific functions in different sub-nuclear compartments and its biological activities are therefore strongly dependent on compartmentalization rather than specificity in the selection of its substrates.

Overall, the rewiring of the RNA-binding protein network increases concomitantly cytosolic and mitochondrial protein synthesis rates (Fig. 8). This switching mechanism probably provides cancer cells with a growth advantage and may therefore be exploited by other oncogenic noncoding RNAs and/or proteins. It will therefore be interesting to assess whether similar mechanisms are at play in other types of cancer.

Although it remains to be formally established that its expression is cancer-specific, it is tempting to speculate that *SAMMSON* is expressed exclusively in melanoma cells as a by-product of aberrant RNA biology. A similar example is provided by a protein-coding gene Δ N-Netrin-1, a variant of Netrin-1 produced by transcription from an internal promoter and detectable only in cancer cells⁴⁶. In contrast with the Netrin-1 protein, which is secreted, the cancer variant localizes aberrantly to the nucleoli where it affects rRNA processing and nucleolar structure⁴⁶. Here we show that *SAMMSON* aberrant expression is sufficient to impose CARF binding to p32, stimulate cytosolic and mitochondrial translation and enhance malignancy in a lineage-independent manner. *SAMMSON* could therefore be viewed as a selfish gene, which tries to perpetuate its expression by increasing proliferation of malignant cells through increased translation.

Together we showed that the oncogenic lncRNA *SAMMSON* hijacks key RNA-binding proteins to concertedly enhance translation in the cytosol and in the mitochondria. This ensures the maintenance of the equilibrium between the two translation rates, which is so essential for cancer cell survival. Targeting this equilibrium through inhibition of mitochondrial protein synthesis machinery is emerging as a promising antimelanoma strategy.

Online content

Any methods, additional references, Nature Research reporting summaries, source data, statements of data availability and associated accession codes are available at <https://doi.org/10.1038/s41594-018-0143-4>.

Received: 27 November 2017; Accepted: 12 September 2018;
Published online: 29 October 2018

References

- Vander Heiden, M. G., Cantley, L. C. & Thompson, C. B. Understanding the Warburg Effect: the metabolic requirements of cell proliferation. *Science* (80-). **324**, 1029–1033 (2009).
- Wang, M. & Pestov, D. G. 5'-end surveillance by Xrn2 acts as a shared mechanism for mammalian pre-rRNA maturation and decay. *Nucleic Acids Res.* **39**, 1811–1822 (2011).
- Teng, T., Thomas, G. & Mercer, C. A. Growth control and ribosomopathies. *Curr. Opin. Genet. Dev.* **23**, 63–71 (2013).
- Wu, H., Sun, H., Liang, X., Lima, W. F. & Crooke, S. T. Human RNase H1 is associated with protein P32 and is involved in mitochondrial pre-rRNA processing. *PLoS ONE* **8**, e71006 (2013).
- Ruggero, D. & Pandolfi, P. P. Does the ribosome translate cancer?. *Nat. Rev. Cancer* **3**, 179–192 (2003).
- Mayer, C. & Grummt, I. Ribosome biogenesis and cell growth: mTOR coordinates transcription by all three classes of nuclear RNA polymerases. *Oncogene* **25**, 6384–6391 (2006).
- Yang, L. et al. Regulation of SirT1-nucleomethylin binding by rRNA coordinates ribosome biogenesis with nutrient availability. *Mol. Cell. Biol.* **33**, 3835–3848 (2013).
- Nishimura, K. et al. Perturbation of ribosome biogenesis drives cells into senescence through 5S RNP-mediated p53 activation. *Cell Rep.* **10**, 1310–1323 (2015).
- Schmidt, O., Pfanner, N. & Meisinger, C. Mitochondrial protein import: from proteomics to functional mechanisms. *Nat. Rev. Mol. Cell Biol.* **11**, 655–667 (2010).
- Fogal, V. et al. Mitochondrial p32 protein is a critical regulator of tumor metabolism via maintenance of oxidative phosphorylation. *Mol. Cell. Biol.* **30**, 1303–1318 (2010).
- Skrčić, M. et al. Inhibition of mitochondrial translation as a therapeutic strategy for human acute myeloid leukemia. *Cancer Cell.* **20**, 674–688 (2011).
- D'Andrea, A. et al. The mitochondrial translation machinery as a therapeutic target in Myc-driven lymphomas. *Oncotarget* **7**, 72415–72430 (2016).
- Battersby, B. J. & Richter, U. Why translation counts for mitochondria – retrograde signalling links mitochondrial protein synthesis to mitochondrial biogenesis and cell proliferation. *J. Cell. Sci.* **126**, 4331–4338 (2013).
- Wang, X. & Chen, X. J. A cytosolic network suppressing mitochondria-mediated proteostatic stress and cell death. *Nature* **524**, 481–484 (2015).
- Wrobel, L. et al. Mistargeted mitochondrial proteins activate a proteostatic response in the cytosol. *Nature* **524**, 485–488 (2015).
- Rosenwald, I. B. The role of translation in neoplastic transformation from a pathologist's point of view. *Oncogene* **23**, 3230–3247 (2004).
- Ruggero, D. The role of Myc-induced protein synthesis in cancer. *Cancer Res.* **69**, 8839–8843 (2009).
- Fogal, V. et al. Mitochondrial p32 is upregulated in Myc expressing brain cancers and mediates glutamine addiction. *Oncotarget* **6**, 1157–1170 (2015).
- Leucci, E. et al. Melanoma addiction to the long non-coding RNA SAMMSON. *Nature* **531**, 518–522 (2016).
- Tollervey, D. Termination by torpedo. *Nature* **432**, 456–457 (2004).
- Watanabe, K. et al. Degradation of initiator tRNAMet by Xrn1/2 via its accumulation in the nucleus of heat-treated HeLa cells. *Nucleic Acids Res.* **41**, 4671–4685 (2013).
- Watanabe, K., Ijiri, K. & Ohtsuki, T. MTOR regulates the nucleoplasmic diffusion of Xrn2 under conditions of heat stress. *FEBS Lett.* **588**, 3454–3460 (2014).
- Petfalski, E., Dandekar, T., Henry, Y. & Tollervey, D. Processing of the precursors to small nucleolar RNAs and rRNAs requires common components. *Mol. Cell. Biol.* **18**, 1181–1189 (1998).
- Henras, A. K., Plisson-Chastang, C., O'Donohue, M. F., Chakraborty, A. & Gleizes, P. E. An overview of pre-ribosomal RNA processing in eukaryotes. *Wiley Interdiscip. Rev. RNA* **6**, 225–242 (2015).
- Preti, M. et al. Gradual processing of the ITS1 from the nucleolus to the cytoplasm during synthesis of the human 18S rRNA. *Nucleic Acids Res.* **41**, 4709–4723 (2013).
- Sato, S. et al. Collaborator of alternative reading frame protein (CARF) regulates early processing of pre-ribosomal RNA by retaining XRN2 (5'-3' exoribonuclease) in the nucleoplasm. *Nucleic Acids Res.* **43**, 10397–10410 (2015).
- Gupta, P. B. et al. The melanocyte differentiation program predisposes to metastasis after neoplastic transformation. *Nat. Genet.* **37**, 1047–1054 (2005).
- Boshuizen, J. et al. Cooperative targeting of melanoma heterogeneity with an AXL antibody-drug conjugate and BRAF/MEK inhibitors. *Nat. Med.* **24**, 203–212 (2018).
- Tripathi, V. et al. The nuclear-retained noncoding RNA MALAT1 regulates alternative splicing by modulating SR splicing factor phosphorylation. *Mol. Cell* **39**, 925–938 (2010).
- Novo, C. et al. The heterochromatic chromosome caps in great apes impact telomere metabolism. *Nucleic Acids Res.* **41**, 4792–4801 (2013).
- Livi, C. M., Klus, P., Delli Ponti, R. & Tartaglia, G. G. CatRAPID signature: identification of ribonucleoproteins and RNA-binding regions. *Bioinformatics* **32**, 773–775 (2015).
- Richter, U. et al. A mitochondrial ribosomal and RNA decay pathway blocks cell proliferation. *Curr. Biol.* **23**, 535–541 (2013).
- West, J. A. et al. The long noncoding RNAs NEAT1 and MALAT1 bind active chromatin sites. *Mol. Cell* **55**, 791–802 (2014).
- Adriaens, C. et al. P53 induces formation of NEAT1 lncRNA-containing paraspeckles that modulate replication stress response and chemosensitivity. *Nat. Med.* **22**, 861–868 (2016).
- Schillewaert, S., Wacheul, L., Lhomme, F. & Lafontaine, D. L. J. The evolutionarily conserved protein Las1 is required for pre-rRNA processing at both ends of ITS2. *Mol. Cell. Biol.* **32**, 430–444 (2012).
- Tollervey, D. & Kiss, T. Function and synthesis of small nucleolar RNAs. *Curr. Opin. Cell Biol.* **9**, 337–342 (1997).
- Weinstein, L. B. & Steitz, J. A. Guided tours: from precursor snoRNA to functional snoRNP. *Curr. Opin. Cell Biol.* **11**, 378–384 (1999).
- Schmidt, E. K., Clavarino, G., Ceppi, M. & Pierre, P. SUnSET, a nonradioactive method to monitor protein synthesis. *Nat. Methods* **6**, 275–277 (2009).
- Pianese, G., Teuscher, R. & Ziegler, E. *Beitrag zur Histologie und Aetiologie des Carcinoms: Histologische und experimentelle Untersuchungen.* (G. Fischer, Jena, Germany, 1896).
- Bywater, M. J. et al. Inhibition of RNA polymerase I as a therapeutic strategy to promote cancer-specific activation of p53. *Cancer Cell.* **22**, 51–65 (2012).
- Quin, J. E. et al. Targeting the nucleolus for cancer intervention. *Biochim. Biophys. Acta* **1842**, 802–816 (2014).
- Silvera, D., Formenti, S. C. & Schneider, R. J. Translational control in cancer. *Nat. Rev. Cancer* **10**, 254–266 (2010).
- Richter-Dennerlein, R., Dennerlein, S. & Rehling, P. Integrating mitochondrial translation into the cellular context. *Nat. Rev. Mol. Cell Biol.* **16**, 586–592 (2015).
- Richter-Dennerlein, R. et al. Mitochondrial protein synthesis adapts to influx of nuclear-encoded protein. *Cell* **167**, 471–483.e10 (2016).
- Richter, U., Lahtinen, T., Marttinen, P., Suomi, F. & Battersby, B. J. Quality control of mitochondrial protein synthesis is required for membrane integrity and cell fitness. *J. Cell. Biol.* **211**, 373–389 (2015).
- Delloye-Bourgeois, C. et al. Nucleolar localization of a netrin-1 isoform enhances tumor cell proliferation. *Sci. Signal.* **5**, ra57–ra57 (2012).
- Bellucci, M., Agostini, F., Masin, M. & Tartaglia, G. G. Predicting protein associations with long noncoding RNAs. *Nat. Methods* **8**, 444–445 (2011).
- Cirillo, D. et al. Quantitative predictions of protein interactions with long noncoding RNAs: to the editor. *Nat. Methods* **14**, 5–6 (2016).

Acknowledgements

GapmeRs were designed by J. Lai (Exiqon, Copenhagen Denmark). We would like to thank M. Leucci for reading and editing the manuscript. This study was supported by the Fund Emile Carpentier—Fund André Vander Stricht—Fund Van Damme 2017-1J810830-207301. The authors wish to thank H. Brems for providing NHEM cultures, A. Sablina (VIB-KULeuven) for providing the SV40 LTA plasmid, M. Spinazzi (VIB-KULeuven) for the technical assistance and for sharing some antibodies, G. Ghanem (Jules Bordet Institute) for the patient-derived melanoma cell line and somersault18:24 (<http://www.somersault1824.com/>) for providing some graphical illustrations. R.V. is a recipient of the FWO PhD fellowship 1S08316N. D.L. is supported by Fonds National de la Recherche (FRS/FNRS). G.G.T.'s research is supported by the European Research Council (grant no. RIBOMYLOME_309545) and the Spanish Ministry of Economy and Competitiveness (grant nos. BFU2014-55054-P and BFU2017-86970-P).

Author contributions

E.L. and R.V. performed most experiments. Y.V. performed experiments described in Fig. 2f. E.N. and K.S. performed the nuclear rRNA northern blot (Fig. 5b and Supplementary Fig. 4a). R.D.P. and A.A. ran the RNA secondary structure prediction and in silico binding (Fig. 4f). P.M. performed the small RNA-seq (Fig. 5d and Supplementary Fig. 4d). H.I. and K.I. performed the experiments in Fig. 4g–i and Supplementary Fig. 4c. L.G. helped with Figs. 5a and 6a and in additional experiments provided to the reviewers and not included in the final manuscript. D.L., G.G.T. and N.T. helped in the interpretation of the data. E.L. and R.V. designed the study. J.C.M. and E.L. wrote the manuscript with input from all the authors.

Competing interests

The authors declare no competing interests.

Additional information

Supplementary information is available for this paper at <https://doi.org/10.1038/s41594-018-0143-4>.

Reprints and permissions information is available at www.nature.com/reprints.

Correspondence and requests for materials should be addressed to E.L.

Publisher's note: Springer Nature remains neutral with regard to jurisdictional claims in published maps and institutional affiliations.

© The Author(s), under exclusive licence to Springer Nature America, Inc. 2018

Methods

Cell culture and transfection. All lines were grown in 5% CO₂ at 37 °C. SK-MEL-28 (a gift from L. Larue), SK-MEL-28 BRAFi resistant (a gift from D. Peeper) and LCLs (a gift from L. Leoncini) were grown in RPMI 1640-glutamax (Gibco, Invitrogen) supplemented with 10% FBS (Gibco, Invitrogen). Mel-ST (a gift from C. Bertolotto) were grown in DMEM-glutamax (Gibco, Invitrogen) supplemented with 7% FBS (Gibco, Invitrogen). HEK293T (from ATCC) were grown in DMEM-glutamax (Gibco, Invitrogen) supplemented with 10% FBS (Gibco, Invitrogen). The patient-derived passages multiple myeloma cell line (a gift from G.-E. Ghanem) were grown in F-10 (Gibco, Invitrogen), supplemented with 10% FBS (Gibco, Invitrogen) and 12 mM Glutamax (Gibco, Invitrogen). NHEM (a gift from H. Brems) were grown in MGM-4 melanocyte growth medium (Lonza). p38 cells were grown in F-12 media (Gibco, Invitrogen) supplemented with 10% FBS (Gibco, Invitrogen), 2 mM Glutamine (Gibco, Invitrogen) and 25 µg ml⁻¹ of Hygromycin B (Thermo Fisher Scientific). All cell lines used in this study were mycoplasma negative.

Cells were transfected with Lipofectamine 2000 (Thermo Fisher Scientific) according to manufacturer instructions with 25 nM of non-targeting GapmeR or SAMMSON-targeting GapmeR3 or 11 (Exiqon) and collected 30 h after transfection, with 25 nM siCARF (SMART-pool, Dharmacom) or with 50 nM of siXRN2 (Sigma-Aldrich) and collected 72 h after transfection. Cells were transfected with Lipofectamine RNAiMax (Thermo Fisher Scientific) according to the manufacturer instructions with 25 nM of siNEAT1 siPOOLS (siTOOLS Biotech) and fixed 72 h after transfection. Sequences of the GapmeRs and siRNAs are indicated in Supplementary Table 1. For HA-XRN2 constructs transfection, four 15 cm Ø plates per construct were transfected with 25 µg plasmid per plate and 70 µl Lipofectamine 2000 per plate and samples were collected 72 h after transfection. HEK293T cells were transfected with standard calcium phosphate method.

Cloning and lentiviral transduction. The SAMMSON-encoding construct was described elsewhere¹⁹. SAMMSON deletion constructs ±RAT-tag were generated as follows. SAMMSON complementary DNA fragment was amplified by a polymerase chain reaction (PCR) using primer sets HIW885 and HIW886 with the SAMMSON-encoding pLenti_PGK_SAMMSON plasmid as a template. The PCR product was ligated into BamH I-Xho I sites of pcDNA5-FRT-TO vector and the resulting product was used for transformation of DH5α competent cells to obtain single clones. Sub-cloned product pcDNA5-FRT-TO-SAMMSON was verified by DNA sequencing. For construction of the RNA aptamer fused with SAMMSON, RAT-tag was amplified by PCR using the primer sets HIW897 and HIW898 with the previously described⁴⁷ RAT-U1 snRNA expression vector as template. Amplified RAT-tag coding fragment was ligated into Xho I-Apa I sites of pcDNA5-FRT-TO-SAMMSON. The resulting product (pcDNA5-FRT-TO-SAMMSON_RAT-tag) was verified by DNA sequencing. Using pcDNA5-FRT-TO-SAMMSON_RAT-tag as a template, SAMMSON deletion mutant coding fragments were amplified by PCR with the following primer sets: HIW885 and HIW899 for SAMMSON-5' half, HIW900 and HIW886 for SAMMSON-3' half, and HIW901 and HIW886 for SAMMSON-3' 500 base, respectively. After removing the full-length SAMMSON sequence from pcDNA5-FRT-TO-SAMMSON_RAT-tag using BamH I-Xho I restriction enzymes, the PCR products were ligated into the same sites. Resultant deletion constructs were verified by DNA sequencing. All primer sequences are indicated in Supplementary Table 1.

HA-XRN2 constructs (WT, C, N1 and N2) were previously described in ref.²⁶. For SAMMSON infection, lentivirus produced in HEK293T cells was used to infect the Mel-ST and LCLs cells. Successfully infected cells were selected in a puromycin (InvivoGen, 0.5 µg ml⁻¹)-containing medium for 1 week. For SV40 LTA (a gift from A. Sablina) infection, lentivirus produced in HEK293T cells was used to infect LCL cells. Successfully infected cells were selected in a hygromycin B (Invitrogen, 100 µg ml⁻¹)-containing medium for 1 week to 2 weeks.

Cell growth and cell death assays. Cell growth was measured with the CellTiter-Glo luminescent cell viability assay (Promega), Caspase activity was measured using the Caspase-Glo 3/7 assay (Promega) with a VIKTOR X4 Reader (PerkinElmer). Tigecycline (Selleck) was used at 5, 25 or 50 µM concentration. BRAFi (Dabrafenib-TAFINLAR, Novartis) and MEKi (Trametinib-MEKINIST, Novartis) were used at 10 nM and 2.5 nM concentrations, respectively. Chloramphenicol (Sigma-Aldrich) was used at a 100, 200 or 400 µg ml⁻¹ concentration.

Cell count, colony assays and soft agar assays. For vital counts, cells were stained with Trypan Blue (Sigma-Aldrich) and counted with TC20 automated cell counter (Biorad).

For colony assays, 1 × 10³ Mel-ST or SK-MEL-28 cells were plated in six-well plates and cultured for 1 week. The cells were then fixed and stained for 15 min with a 1% crystal violet in 35% methanol solution. Chloramphenicol (Sigma-Aldrich) was used at a 100–200–400 µg ml⁻¹ concentration.

For soft agar assay, 1 × 10⁴ cells were embedded in 1 ml of RPMI 1640 containing 10% FBS and 0.35% noble agar (Sigma-Aldrich) on a base layer made of RPMI 1640 containing 10% FBS and 2% noble agar in a well of a six-well plate.

After 2–3 weeks of incubation, cells were fixed and stained with a crystal violet solution (0.05% crystal violet, 0.05% methanol and 0.37% PFA) for 2 h.

RAP-WB. For the validation of protein targets, two sets of 48 tiling probes were used to affinity purify mature SAMMSON and HPRT transcripts (Biosearch Technologies). Briefly, 100 µl of Streptavidin Sepharose High Performance beads (GE Healthcare) were coupled to 400 pmol of biotinylated probes against SAMMSON overnight at 4 °C. Cells (6 × 10⁷ cells per sample) were lysed in 2 ml of pull-out buffer (20 mM Tris-HCl pH 7.5, 200 mM NaCl, 2.5 mM MgCl₂, 0.05% Igepal, 60 U ml⁻¹ Suprase-In (Ambion), 1 mM dithiothreitol (DTT) and 1 × Halt Protease and Phosphatase Inhibitor Single-Use Cocktail (Life Technologies)) and incubated for 3 h with the beads at 4 °C on a rotating wheel. As a negative control, an additional sample was digested with 10 µg ml⁻¹ RNase A for 10 min at room temperature before incubation with SAMMSON probes.

For the crosslinking experiments, cells were washed once in phosphate buffer saline, crosslinked dry at 400 mJ cm⁻² and lysed. Washes were performed in RNase-free water.

RIP. RIP was performed as previously described⁴⁸. p32, XRN2 and CARF were immuno-precipitated using 4 µg of specific antibody (p32, A302-862A, Bethyl Laboratories; XRN2, A301-103A, Bethyl Laboratories; CARF, A303-862A, Bethyl Laboratories) coupled to 35 µl of protein G Dynabeads (Invitrogen) overnight at 4 °C on a rotating wheel.

RIP/RAP efficiency. The relative expression of the genes of interest for the RIP/RAP assays was calculated applying the $\Delta \Delta C_i$ method. In brief, the C_i value of the RIP/RAP was subtracted from the C_i value of the Input for every gene, thus obtaining the ΔC_i for each gene in the RIP/RAP sample. The RIP/RAP ΔC_i was then subtracted from the ΔC_i of the immunoglobulin (IgG), control probe or control sample (WT for Fig. 4c) for every gene, thus obtaining the $\Delta \Delta C_i$. To calculate the fold enrichment, the following equation was applied: fold enrichment = $2^{-\Delta \Delta C_i}$.

RNA aptamer-based affinity purification. To identify p32-CARF-XRN2 binding sites on SAMMSON, the RAT-tag based method was used⁴⁷ with slight modifications. Briefly, a mixture of three plasmids was co-transfected into HEK293T cells; one plasmid expressed RAT-tagged SAMMSON derivatives, one plasmid y18Sn tagged U2 (pcDdCMV-y18Sn-U2⁴⁹) for transfection control and one plasmid expressed HA-FLAG (HF)-tagged PP7CP (pcDNA3.1-PP7CP-HF) in a 7:2:1 ratio. The 24 h post-transfection medium was changed and after 4 h of incubation cells were collected. The cells were then lysed in lysis buffer (50 mM Tris-HCl pH 8.0, 150 mM NaCl, 2.5 mM MgCl₂, 0.5% IGEPAL-CA630, 1 mM phenylmethylsulfonyl fluoride, PMSF) and incubated on ice for 15 min. The soluble fraction, obtained after centrifugation at 20,000 xg for 15 min at 4 °C, was mixed with anti-FLAG-M2-conjugated agarose beads and rotated for 4 h at 4 °C. PP7CP-HF bound to RAT-tagged SAMMSON RNA-protein complexes was captured by the beads. After five washes with lysis buffer and once with lysis buffer without IGEPAL-CA630, RAT-tagged SAMMSON or its derivative bound with its associated proteins were eluted from the beads with 500 µg ml⁻¹ FLAG peptide in the same buffer.

RT-qPCR. RNA was extracted with QIAzol lysis reagent (Qiagen) or with Nucleospin RNA/protein kit (Macherey-Nagel). RNA was reverse transcribed using the High-Capacity complementary DNA Reverse Transcription Kit (Thermo Fisher Scientific). SAMMSON, TERRA, MALAT1, LINC00698, p32, COX1, NDI, 18S, 16S and 12S expression was measured by qPCR on a LightCycler 480 (Roche) and normalized in qbase + 3.0 (Biogazelle) using HPRT1, TBP and UBC as reference genes. Sequences of the primers are indicated in Supplementary Table 1.

Northern blotting. Nuclear pre-rRNA-processing analysis was conducted as previously described³⁰. For northern blot analysis of mitochondrial pre-rRNAs, 4 µg of total RNA was subjected to 0.9% agarose-formaldehyde gel electrophoresis in 3-(N-morpholino)propanesulfonic acid running buffer and the separated RNAs were transferred to a Hybond-N+ membrane (GE Healthcare). The membrane was dried and subsequently crosslinked at 120 mJ cm⁻². After being stained with methylene blue, the membrane was hybridized to biotin-labeled DNA probe at 42 °C overnight in PerfectHyb Plus hybridization buffer (Sigma-Aldrich) according to the manufacturer's instructions. The hybridized membrane was washed sequentially with 2 × sodium lauryl sulfate containing 0.1% sodium dodecyl sulfate at 25 °C for 5 min, 0.5 × sodium lauryl sulfate containing 0.1% sodium dodecyl sulfate at 50 °C for 20 min, and 0.1 × sodium lauryl sulfate containing 0.1% sodium dodecyl sulfate at 25 °C for 20 min. The hybridized RNAs were detected using a Chemiluminescent Nucleic Acid Detection Module kit (Thermo Fisher Scientific) according to the manufacturer's instructions. RNA signals were detected using LAS4000 image analyzer and the signal intensities of RNA bands were quantified by Image J software.

Library preparation, small RNA-seq and data processing. Small RNA libraries were generated using the TruSeq small RNA library prep kit (Illumina) on 100 ng of input RNA according to the manufacturer's instructions. Size selection was

performed using a Pippin prep device (Sage Science). Libraries were quantified using a BioAnalyser (Agilent) and sequenced on a NextSeq500 (Illumina).

Small RNAs were quantified using Biogazelle's dedicated small RNA-seq pipeline (part of Cobra). Adaptors were trimmed using Cutadapt, discarding reads shorter than 15 nt and reads without adaptors.

Read quality was evaluated using the FASTX-Toolkit, applying a minimum quality score of 20 in at least 80% of bases. Reads were mapped using Bowtie without allowing mismatches. Mapped reads were subsequently annotated by matching genomic coordinates of each read with genomic locations of miRNAs (obtained from miRBase, v20⁵¹) and other small RNAs (obtained from UCSC and Ensembl^{52,53}).

SUNSET. SUNSET was performed as described³⁵. Briefly, ~80% confluent cells were washed twice in 1× phosphate buffer saline and subsequently pulsed with puromycin-containing media (InvivoGen, 10 µg ml⁻¹) for 10 min. Due to the fact that puromycin is a structural analogue of aminoacyl tRNAs, it gets incorporated into the nascent polypeptide chain and prevents elongation. Thus, when used for reduced amounts of time, puromycin incorporation in neosynthesized proteins directly reflects the rate of mRNA translation in vitro. Puromycin incorporation was measured by western blotting using an antibody that recognizes puromycin.

Click-iT metabolic labeling for protein. Click-iT protein labeling (Invitrogen) was performed according to the manufacturer's instruction. Cells were incubated for 1 h in methionine-free medium. Afterwards, 50 µM L-azidohomoalanine were added to the media for 3 h. The signal was detected using an horseradish peroxidase- (HRP)-conjugated streptavidin antibody (ab7403, Abcam, 1:20,000).

Cellular fractionation and mitoplast isolation. Briefly, mitochondria were purified from 4–6 × 10⁷ cells using mitochondria isolation kit for cultured cells (Thermo Fisher Scientific) according to manufacturer instructions, all buffers were supplemented with 60 U ml⁻¹ Superase-In (Ambion) and 1× Halt Protease and Phosphatase Inhibitor Single-Use Cocktail (Life Technologies). Mitoplasts were obtained by incubating purified mitochondria in RNase A-containing hypotonic buffer (HEPES pH 7.2 supplemented with 1× Halt Protease and Phosphatase Inhibitor Single-Use Cocktail (Life Technologies) and 10 µg ml⁻¹ RNase A (Roche)) for 20 min on ice and subsequently incubated for an additional 10 min at room temperature to remove all possible RNA contaminants. The purified mitoplasts were then washed three times with Mitoplast Isolation Buffer (250 mM Mannitol, 5 mM HEPES pH 7.2, 0.5 mM EGTA, 1 mg ml⁻¹ bovine serum albumin (BSA) supplemented with 60 U ml⁻¹ Superase-In (Ambion) and 1× Halt Protease and Phosphatase Inhibitor Single-Use Cocktail (Life Technologies)). For proteinase K experiments, purified mitochondria were resuspended in 1× sucrose buffer (HEPES 10 mM, sucrose 280 mM, EGTA 1 mM pH 7.4) supplemented with 100 µg ml⁻¹ proteinase K (Sigma-Aldrich) and with 60 U ml⁻¹ Superase-In (Ambion) for 30 min at 4°C rotating. Mitochondria were then pelleted at 9,000g for 10 min. Afterwards, mitochondria were resuspended in 1× sucrose buffer supplemented with 20 nM PMSF (Sigma-Aldrich) and with 60 U ml⁻¹ Superase-In (Ambion) and pelleted at 9,000g for 10 min. An additional washing step was performed with 1× sucrose buffer supplemented with 20 nM PMSF (Sigma-Aldrich) and 1× Halt Protease and Phosphatase Inhibitor Single-Use Cocktail (Life Technologies) and with 60 U ml⁻¹ Superase-In (Ambion). RNA and protein were then extracted with Nucleospin RNA/protein kit (Macherey-Nagel). Mitochondria and mitoplast enrichment was validated by RT-qPCR for the 16S mt-rRNA and by western blot using antibodies directed against multiple mitochondrial proteins and calreticulin or calnexin (to exclude the possibility of endoplasmic reticulum contaminants). The same amount of proteins was loaded on the gel for each fraction to compare the enrichment of the different fractions.

Antibodies. Western blotting experiments were performed using the following primary antibodies: vinculin (V9131, clone hVIN-1 Sigma-Aldrich, 1:10,000), GAPDH (ab9485, Abcam, 1:1,000 or AM4300, clone 6C5, Ambion, 1:20,000), β-actin (sc-69879, clone AC-15, Santa Cruz Biotechnology, 1:2,000), p32 (A302-863A, Bethyl Laboratories, 1:5,000 or sc-10258, clone D-19, Santa Cruz Biotechnology, 1:1,000), XRN2 (A301-103A, Bethyl Laboratories, 1:2,000), CARF (A303-861A, Bethyl Laboratories, 1:2,000), NDUFS3 (Abcam 14711, 1:1,000), VDAC1 (ab3434-100, Abcam, 1:2,000), Hsp60 (BD611562, BD Biosciences, 1:5,000), Tom20 (FL-145, sc-11415, Santa Cruz Biotechnology, 1:1,000), calreticulin (C4606, Sigma-Aldrich, 1:10,000), calnexin (ab22595, Abcam, 1:5,000), SRSF1 (32-4600, Thermo Fisher Scientific, 1:250), puromycin (MABE343, clone 12D10, Merck Millipore, 1:25,000) and HA-tag (3724, clone C29F4, Cell Signaling Technologies, 1:1,000). The following HRP-linked secondary antibodies were used: anti-goat IgG (A5420, Sigma-Aldrich, 1:10,000), anti-mouse IgG (7076S, Cell Signaling Technologies, 1:5,000) and anti-rabbit IgG (NA934-1ML, Sigma-Aldrich, 1:10,000).

Fluorescence in situ hybridization (FISH). For detection of *NEAT1* and the 12S at a single-cell level, pools of FISH probes were designed using the Stellaris probe

designer software (Biosearch Technologies). Cells were grown on eight-well slides and fixed in 3.7% formaldehyde and permeabilized in 70% EtOH for >15 min at 4°C. Hybridization was carried out overnight at 37°C in 2× sodium lauryl sulfate, 10% formamide and 10% dextran. Cells were counterstained with 4,6-diamidino-2-phenylindole (DAPI) and visualized using an Olympus Fluoview FV1200 using a LD635 laser for Cy5, LD559 HeNe for Cy3.5 and LD405 for DAPI.

Immunofluorescence. For immunofluorescence, cells were grown on eight-well slides, fixed in 3.7% formaldehyde and permeabilized in 1% BSA (Sigma-Aldrich) and 0.2% Triton X-100 (Sigma-Aldrich)-containing buffer for 10 min on ice. Blocking was performed in 1% BSA and 10% goat serum (DAKO) for 30 min at room temperature. Primary antibody incubation was performed at room temperature for 1 h. To detect p32, a rabbit antibody (A302-863A) from Bethyl Laboratories was used at a concentration of 1:1,000. To detect XRN2, a rabbit antibody (A301-103A) from Bethyl Laboratories was used at a concentration of 1:250. To detect CARF, a mouse antibody (H00055602-B01P) from Abnova was used at a concentration of 1:200. To detect puromycin, a mouse antibody (MABE343, clone 12D10) from Merck Millipore was used at a concentration of 1:10,000. To detect fibrillar, a mouse antibody (ABIN361375, clone 38F3) from Anticorps was used at a concentration of 1:500. Secondary antibody incubation was performed for 45 min at room temperature in the dark. As secondary antibodies, anti-rabbit or anti-mouse AlexaFluor-488 and AlexaFluor-647 (Life Technologies, 1:1,000) were used. MitoTracker™ Red CMXRos (Thermo Fisher Scientific) was added to the cells at a final concentration of 300 nM 30 min prior to fixation. Slides were then mounted with ProLong Gold Antifade Mountant with DAPI (Thermo Fisher Scientific). Images were analyzed on an Olympus Fluoview FV1200 using a LD635 laser for Cy5, LD559 HeNe for Cy3.5 and LD405 for DAPI.

Proximity ligation assay (PLA). PLA Duolink FarRed (Sigma-Aldrich) was performed following the manufacturer's instructions. To detect p32, a rabbit antibody (A302-863A) from Bethyl Laboratories was used at a concentration of 1:1,000. To detect CARF, a mouse antibody (H00055602-B01P) from Abnova was used at a concentration of 1:200. PLA Probe Anti-Rabbit PLUS and PLA Probe Anti-Mouse MINUS were used.

Xenografts. Animals were housed under pathogen-free conditions. All procedures involving animals (NMRI, female, 4 weeks old) were performed in accordance with the guidelines of the Catholic University of Leuven (KU Leuven) Animal Care and Use Ethical Committee (P147/2012). At the age of 4 weeks, mice were injected subcutaneously in either one or both flanks with 5 × 10⁶ Mel-ST cells in 100 µl serum-free medium. Tumor volumes were calculated with the formula $L \times W \times H \times 0.52$, where L is length, W is width and H is height.

Immunohistochemistry. Tumor samples were fixed in 3.7% PFA for 24 h at 4°C, dehydrated with 70% EtOH for 24 h at 4°C and subsequently rehydrated with demineralized water. The samples were then cut in sections of about 4 µm. Specimens were stained with haematoxylin and eosin and immunohistochemistry was performed using microwave pre-treatment of slides for antigen retrieval. Antibodies against Ki-67 (SP6, Thermo Fisher Scientific RM-9106-S, clone SP6, 1:200) and puromycin (Merck Millipore, clone 12D10, 1:15,000) were applied, in conjunction with goat anti-rabbit HRP-conjugated antibodies (DAKO) and visualized by DAB reaction. To evaluate the stainings, positive cells were counted using ImageJ.

RNA-protein interactions (catRAPID). Interactions of SAMMSON to XRN2, CARF and p32 were predicted using catRAPID^{54,55}, an algorithm that computes RNA-protein interactions by combining secondary structure, hydrogen bonding and van der Waals contributions. Background correction was obtained by subtracting the profile of AQP1, a bona fide negative control, not retrieved in the mass spectrometry data from SAMMSON pulldown.

Statistical analysis. The significance between means was determined by two-tailed paired Student's t -test, with the exception of Fig. 6b where two-way analysis of variation (ANOVA) was used and of Supplementary Fig. 8c where a two-tailed unpaired Student's t -test was used. P values are represented as $P > 0.05$, not significant (NS); $P < 0.05$, *; $P < 0.01$, **; $P < 0.001$, ***; $P < 0.0001$, ****. All statistical analyses were performed with GraphPad Prism v7.0a (April 2, 2016) for Mac OS X.

Reporting Summary. Further information on research design is available in the Nature Research Reporting Summary linked to this article.

Data availability

Small RNA sequencing data have been submitted to the Sequence Read Archive under accession code [SRP151840](https://www.ncbi.nlm.nih.gov/sra/SRP151840). Source data and statistical analysis for Figs. 1a,b,d,e, 2a,c,e,f, 3a,d,f,h, 4c,e, 5c, 6d,g,h and 7b–g are available in the Supplementary Information online. All other data that support the findings of this study are available from the corresponding author upon reasonable request.

References

49. Ishikawa, H. et al. Identification of truncated forms of U1 snRNA reveals a novel RNA degradation pathway during snRNP biogenesis. *Nucleic Acids Res.* **42**, 2708–2724 (2014).
50. McHugh, C. A. et al. The Xist lncRNA interacts directly with SHARP to silence transcription through HDAC3. *Nature* **521**, 232–236 (2015).
51. Ishikawa, H. et al. Truncated forms of U2 snRNA (U2-tfs) are shunted toward a novel uridylylation pathway that differs from the degradation pathway for U1-tfs. *RNA Biol.* **15**, 261–268 (2018).
52. Tafforeau, L. et al. The complexity of human ribosome biogenesis revealed by systematic nucleolar screening of pre-rRNA processing factors. *Mol. Cell* **51**, 539–551 (2013).
53. Kozomara, A. & Griffiths-Jones, S. MiRBase: annotating high confidence microRNAs using deep sequencing data. *Nucleic Acids Res.* **42**, D68–D73 (2014).
54. Speir, M. L. et al. The UCSC Genome Browser database: 2016 update. *Nucleic Acids Res.* **44**, D717–D725 (2016).
55. Yates, A. et al. Ensembl 2016. *Nucleic Acids Res.* **44**, D710–D716 (2016).

Life Sciences Reporting Summary

Nature Research wishes to improve the reproducibility of the work that we publish. This form is intended for publication with all accepted life science papers and provides structure for consistency and transparency in reporting. Every life science submission will use this form; some list items might not apply to an individual manuscript, but all fields must be completed for clarity.

For further information on the points included in this form, see [Reporting Life Sciences Research](#). For further information on Nature Research policies, including our [data availability policy](#), see [Authors & Referees](#) and the [Editorial Policy Checklist](#).

Please do not complete any field with "not applicable" or n/a. Refer to the help text for what text to use if an item is not relevant to your study. For final submission: please carefully check your responses for accuracy; you will not be able to make changes later.

▶ Experimental design

1. Sample size

Describe how sample size was determined.

Sample size was determined empirically. No statistical methods were used to predetermine sample size.

For animal experiments, a pilot study was run to assess the tumor-forming capacity and the latency of the cells at three different cell concentrations. Based on those results (100% of tumor growth regardless of the concentration), n=8 was chosen to assess whether an effect was present.

2. Data exclusions

Describe any data exclusions.

No data were excluded from the analyses.

3. Replication

Describe the measures taken to verify the reproducibility of the experimental findings.

All experiments were performed at least in three independent biological replicates. Reagents were freshly prepared for every experiment and different batches of reagents were used for separate biological replicates. Some experiments were independently run by two different people to corroborate the findings. The number of replicates is indicated for each experiment.

4. Randomization

Describe how samples/organisms/participants were allocated into experimental groups.

For cell lines undergoing a treatment, cells were plated from the same aliquot at the same density and subsequently treated accordingly.

For lentiviral infection, cells were infected at the same time with empty or GOI-encoding plasmid with virus with the same m.o.i. produced on the same day. Only cells infected at the same time were used for each experiment. For biological replicates, cells infected with different batches of virus were used.

For mice experiments, mice were injected with cells infected with an empty construct on one flank and with the GOI-carrying construct on the other flank.

5. Blinding

Describe whether the investigators were blinded to group allocation during data collection and/or analysis.

Form mouse studies, no blinding was needed since both conditions were injected in the same mouse. To document the findings, pictures of each tumor (containing a unit of measure) were taken.

Note: all in vivo studies must report how sample size was determined and whether blinding and randomization were used.

6. Statistical parameters

For all figures and tables that use statistical methods, confirm that the following items are present in relevant figure legends (or in the Methods section if additional space is needed).

n/a Confirmed

- The exact sample size (n) for each experimental group/condition, given as a discrete number and unit of measurement (animals, litters, cultures, etc.)
- A description of how samples were collected, noting whether measurements were taken from distinct samples or whether the same sample was measured repeatedly
- A statement indicating how many times each experiment was replicated
- The statistical test(s) used and whether they are one- or two-sided
Only common tests should be described solely by name; describe more complex techniques in the Methods section.
- A description of any assumptions or corrections, such as an adjustment for multiple comparisons
- Test values indicating whether an effect is present
Provide confidence intervals or give results of significance tests (e.g. P values) as exact values whenever appropriate and with effect sizes noted.
- A clear description of statistics including central tendency (e.g. median, mean) and variation (e.g. standard deviation, interquartile range)
- Clearly defined error bars in all relevant figure captions (with explicit mention of central tendency and variation)

See the web collection on [statistics for biologists](#) for further resources and guidance.

► Software

Policy information about [availability of computer code](#)

7. Software

Describe the software used to analyze the data in this study.

All analyses were performed with GraphPad Prism v7.0a (April 2, 2016) for Mac OS X.

For manuscripts utilizing custom algorithms or software that are central to the paper but not yet described in the published literature, software must be made available to editors and reviewers upon request. We strongly encourage code deposition in a community repository (e.g. GitHub). *Nature Methods* [guidance for providing algorithms and software for publication](#) provides further information on this topic.

► Materials and reagents

Policy information about [availability of materials](#)

8. Materials availability

Indicate whether there are restrictions on availability of unique materials or if these materials are only available for distribution by a third party.

All materials and reagents are available from standard commercial sources.
DNA constructs are available from the authors upon reasonable requests.

9. Antibodies

Describe the antibodies used and how they were validated for use in the system under study (i.e. assay and species).

The following primary antibodies were used: vinculin (V9131, clone hVIN-1, Sigma-Aldrich, LOT#129K484P), GAPDH (ab9485, Abcam, LOT#GR301708-1 and 6C5, AM4300, Ambion, LOT#00326548), b-actin (AC-15, sc-69879, Santa Cruz Biotechnology, LOT#K1715), p32 (A302-863A, Bethyl Laboratories, no LOT# provided; A302-862A, Bethyl Laboratories, no LOT# provided and D-19, sc-10258, Santa Cruz Biotechnology, LOT#D3004), XRN2 (A301-103A, Bethyl Laboratories, no LOT# provided), CARF (A303-861A, Bethyl Laboratories, no LOT# provided; A303-862A, Bethyl Laboratories, no LOT# provided; H00055602-B01P, Abnova, LOT#10252), NDUFS3 (Abcam 14711, LOT#GR192954-4), VDAC1 (ab3434-100, Abcam, LOT#GR103383-1), Hsp60 (BD611562, BD Biosciences, LOT# not available), Tom20 (sc-11415, Santa Cruz Biotechnology, LOT# not available), calreticulin (C4606, Sigma-Aldrich), calnexin (ab22595, Abcam, LOT# not available), puromycin (MABE343, clone 12D10, Merck-Millipore, LOT#2672968), SRSF1 (32-4600, Thermo Fisher Scientific, LOT#RFC34850), HA-tag (3724, clone C29F4, Cell Signaling Technologies, LOT#7, REF 09/2015), fibrillarin, (ABIN361375, clone 38F3, Anticorps, LOT#GS1114b), Ki-67 (SP6, Thermo Fisher Scientific #RM-9106-S, clone SP6, LOT#9106RQ1509B). The following HRP-linked secondary antibodies were used: anti-goat IgG (A5420, Sigma-Aldrich, LOT# not available), anti-mouse IgG (7076S, Cell Signaling Technologies, LOT#32 03/2016), anti-rabbit IgG (NA934-1ML, Sigma-Aldrich, LOT#16803301). The following fluorescent goat cross-adsorbed secondary antibodies were used: anti-mouse Alexa Fluor 488 (A11001, Thermo Fisher Scientific, LOT#17525114), anti-mouse Alexa Fluor 647 (A21235, Thermo Fisher Scientific, LOT#1786359), anti-rabbit Alexa Fluor 488 (A11008, Thermo Fisher Scientific, LOT#1885240), anti-rabbit Alexa Fluor 647 (A21246, Thermo Fisher Scientific, LOT#1596041). The dilutions of the different antibodies were described in the Materials & Methods section. Information regarding validation, citations, and antibody profiles are available on the manufacturer's website. XRN2, p32 and CARF antibodies were further validated by KD with siRNAs followed by western blotting and IF. VDAC1, NDUFS3, Hsp60, Tom20, vinculin, GAPDH, calreticulin and calnexin were validated by cellular fractionation followed by western blotting. Fibrillarin was validated by immunofluorescence. HA-tag was validated by using positive and negatives controls. Puromycin was validated both in vitro and in vivo by western blotting, immunofluorescence and ICH using positive and negatives controls.

10. Eukaryotic cell lines

a. State the source of each eukaryotic cell line used.

SK-MEL-28, provider: Lionel Larue.
SK-MEL-28 BRAFi resistant, provider: Daniel Peeper.
Raji, provider: Lorenzo Leoncini.
LCLs, provider: Lorenzo Leoncini.
Mel-ST, provider: Corine Bertolotto.
HEK293T, provider: ATCC.
p38, provider: ATCC.
MM cell lines, provider: Ghanem-Elias Ghanem.
NHEM, provider: KU Leuven Dpt. Human Genetics.

b. Describe the method of cell line authentication used.

All cell lines were routinely tested by RT-qPCR and western blot using cell type-specific markers.

c. Report whether the cell lines were tested for mycoplasma contamination.

All cell lines were frequently tested for mycoplasma contamination and were always found negative.

d. If any of the cell lines used are listed in the database of commonly misidentified cell lines maintained by [ICLAC](#), provide a scientific rationale for their use.

No commonly misidentified cell lines were used.

► Animals and human research participants

Policy information about [studies involving animals](#); when reporting animal research, follow the [ARRIVE guidelines](#)

11. Description of research animals

Provide all relevant details on animals and/or animal-derived materials used in the study.

Species: *Mus Musculus*.
Strain: NMRI nude mice (BomTac:NMRI-Foxn1nu).
Sex: females.
Age: 4 weeks (start of the experiment)-12 weeks (end of the experiment).

Policy information about [studies involving human research participants](#)

12. Description of human research participants

Describe the covariate-relevant population characteristics of the human research participants.

This study did not involve human participants.